Complete next-to-leading order perturbative QCD prediction for the pion electromagnetic form factor

B. Melić,* B. Nižić,† and K. Passek‡
Theoretical Physics Division, Rudjer Bošković Institute, P.O. Box 1016, HR-10001 Zagreb, Croatia
(Received 2 February 1998; revised manuscript received 25 March 1999; published 24 August 1999)

We present the results of a complete leading-twist next-to-leading order (NLO) QCD analysis of the spacelike pion electromagnetic form factor at large momentum transfer Q. We have studied their dependence on the form of the pion distribution amplitude. For a given distribution amplitude, we have examined the sensitivity of the predictions to the choice of the renormalization and factorization scales. Compared to the renormalization scale, the factorization scale turns out to be of secondary importance. The renormalization scale dependence of the leading-order (LO) results has been significantly reduced by including the NLO corrections. Adopting the criteria according to which a NLO prediction is considered reliable if both the ratio of the NLO to LO contributions and the strong coupling constant are reasonably small, we find that reliable perturbative predictions for the pion electromagnetic form factor with all distribution amplitudes considered can already be made at a momentum transfer Q of the order $5-10$ GeV, with corrections to the LO results being up to $\sim 30\%$. The theoretical uncertainty related to the renormalization scale ambiguity has been estimated to be less than 10%. To check our predictions and to discriminate between the distribution amplitudes, it is necessary to obtain experimental data extending to higher values of Q. [S0556-2821(99)03315-9]

PACS number(s): 13.40.Gp, 12.38.Bx

I. INTRODUCTION

Exclusive processes involving large momentum transfer are among the most interesting and challenging tests of quantum chromodynamics (QCD).

The framework for analyzing such processes within the context of perturbative QCD (PQCD) has been developed by Brodsky and Lepage [1], Efremov and Radyushkin [2], and Duncan and Mueller [3] (see Ref. [4] for reviews). They have demonstrated, to all orders in perturbation theory, that exclusive amplitudes involving large momentum transfer factorize into a convolution of a process-independent and perturbatively incalculable distribution amplitude, one for each hadron involved in the amplitude, with a process-dependent and perturbatively calculable hard-scattering amplitude.

Within the framework developed in Refs. [1–3], leading-order (LO) predictions have been obtained for many exclusive processes. It is well known, however, that, unlike in QED, the LO predictions in PQCD do not have much predictive power, and that higher-order corrections are essential for many reasons. In general, they have a stabilizing effect reducing the dependence of the predictions on the schemes and scales. Therefore, to achieve a complete confrontation between theoretical predictions and experimental data, it is very important to know the size of radiative corrections to the LO predictions. The list of exclusive processes at large momentum transfer analyzed at next-to-leading order (NLO) is very short and includes only three processes: the pion electromagnetic form factor [5–10], the pion transition form factor [10–12], and photon-photon annihilation into two flavor-nonsinglet helicity-zero mesons, $\gamma\gamma \to M\overline{M}$ $(M=\pi,\ K)$ [13].

In leading twist, the pion electromagnetic form factor (the simplest exclusive quantity) can be written as

$$F_\pi(Q^2) = \int_0^1 dx \int_0^1 dy \times \Phi^*(y,\mu_F^2) T_H(x,y,Q^2,\mu_R^2,\mu_F^2) \Phi(x,\mu_F^2). \quad (1.1)$$

Here $\Phi(x,\mu_F^2)$ is the pion distribution amplitude, i.e., the probability amplitude for finding the valence $q_1\overline{q}_2$ Fock state in the initial pion with the constituents carrying the longitudinal momentum xP and $(1-x)P$; $T_H(x,y,Q^2,\mu_R^2,\mu_F^2)$ is the hard-scattering amplitude, i.e., the amplitude for a parallel $q_1\overline{q}_2$ pair of the total momentum P hit by a virtual photon γ^* of momentum q to end up as a parallel $q_1\overline{q}_2$ pair of momentum $P'=P+q$; $\Phi^*(y,\mu_F^2)$ is the amplitude for the final state $q_1\overline{q}_2$ to fuse back into a pion; $Q^2=-q^2$ is the momentum transfer in the process and is supposed to be large; μ_R is the renormalization (or coupling constant) scale and μ_F is the factorization (or separation) scale at which soft and hard physics factorize.

The hard-scattering amplitude T_H can be calculated in perturbation theory and represented as a series in the QCD running coupling constant $\alpha_S(\mu_R^2)$. The function Φ is intrinsically nonperturbative, but its evolution can be calculated perturbatively.

Although the PQCD approach of Refs. [1–3] undoubtedly represents an adequate and efficient tool for analyzing exclusive processes at very large momentum transfer, its applicability to these processes at experimentally accessible momentum transfer has long been debated and attracted much

*Electronic address: melic@thphys.irb.hr
†Electronic address: nizic@thphys.irb.hr
‡Electronic address: passek@thphys.irb.hr

attention. The concern has been raised [14,15] that, even at very large momentum transfer, important contributions to these processes can arise from nonfactorizing end-point contributions of the distribution amplitudes with $x \sim 1$. It has been shown, however, that the incorporation of the Sudakov suppression effectively eliminates these soft contributions and that the PQCD approach to the pion form factor begins to be self-consistent for a momentum transfer of about $Q^2 > 4$ GeV^2 [16] (see also Ref. [17]).

To obtain the complete NLO prediction for the pion form factor requires calculating NLO corrections to both the hard-scattering amplitude and the evolution kernel for the pion distribution amplitude.

The NLO predictions for the pion form factor obtained in Refs. [5–9] are incomplete insofar as only the NLO correction to the hard-scattering amplitude has been considered, whereas the corresponding NLO corrections to the evolution of the pion distribution amplitude have been ignored. Apart from not being complete, the results of the calculations presented in Refs. [5–9] do not agree with one another.

Evolution of the distribution amplitude can be obtained by solving the differential-integral evolution equation using the moment method. In order to determine the NLO corrections to the evolution of the distribution amplitude, it is necessary to calculate two-loop corrections to the evolution kernel. These have been computed by different authors and the obtained results are in agreement [18]. Because of the complicated structure of these corrections, it is possible to obtain numerically only the first few moments of the evolution kernel [19]. Using these incomplete results, the first attempt to include the NLO corrections to the evolution of the distribution amplitude in the NLO analysis of the pion form factor was obtained in Ref. [10]. It has been found that the NLO corrections to the evolution of the pion distribution amplitude as well as to the pion form factor are tiny.

Considerable progress has recently been made in understanding the NLO evolution of the pion distribution amplitude [20]. Using conformal constraints, the complete formal solution of the NLO evolution equation has been obtained. Based on this result, it has been found that, contrary to the estimates given in Ref. [10], the NLO corrections to the evolution of the distribution amplitude are rather large. It has been concluded that because of the size of the discovered corrections, and their dependence upon the input distribution amplitude, the evolution of the distribution amplitude has to be included in the NLO analysis of exclusive processes at large momentum transfer.

The purpose of this paper is to present a complete leading-twist NLO QCD analysis of the spacelike pion electromagnetic form factor at large momentum transfer.

The plan of the paper is as follows. To check and verify the results obtained in Refs. [5–9], in Sec. II we carefully calculate all one-loop diagrams contributing to the NLO hard-scattering amplitude for the pion form factor. We use the Feynman gauge, the dimensional regularization method, and the modified minimal-subtraction ($\overline{\rm MS}$) scheme. Our results are in agreement with those obtained in Refs. [5] (modulo typographical errors listed in [9]) and [7]. Making use of the method introduced in Ref. [20], in Sec. III we determine NLO evolutional corrections to four available candidate pion distribution amplitudes. In Sec. IV we discuss several possible choices of the renormalization scale μ_R and the factorization scale μ_F. In Sec. V we obtain complete NLO numerical predictions for the pion form factor using the four candidate pion distribution amplitudes. For a given distribution amplitude we examine the sensitivity of the predictions on the renormalization and factorization scales, μ_R and μ_F, respectively. We take $\Lambda_{\overline{\rm MS}} = 0.2$ GeV for the calculation presented here. Section VI is devoted to discussions and some concluding remarks.

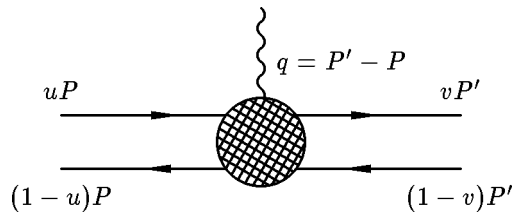

FIG. 1. Feynman diagrams describing the $(q_1\bar{q}_2) + \gamma^* \to (q_1\bar{q}_2)$ transition amplitude in terms of which the hard-scattering amplitude for the pion form factor is obtained.

II. NLO CORRECTION TO THE HARD-SCATTERING AMPLITUDE

In this section we recalculate the NLO correction to the hard-scattering amplitude for the pion form factor.

In leading twist, the hard-scattering amplitude is obtained by evaluating the $(q_1\bar{q}_2) + \gamma^* \to (q_1\bar{q}_2)$ amplitude, which is described by the Feynman diagrams in Fig. 1, with massless valence quarks collinear with parent mesons. In this figure, uP and $(1-u)P$ [vP' and $(1-v)P'$] denote the longitudinal momenta of the pion constituents before the subtraction of collinear singularities. In this evaluation, terms of order m^2/Q^2 are not included and, since the constituents are constrained to be collinear, terms of order $k_\perp^2/Q^2$ ($k_\perp$ is the average transverse momentum in the meson) are not taken into account either. By projecting the $q_1\bar{q}_2$ pair into a color-singlet pseudoscalar state the amplitude corresponding to any of the diagrams in Fig. 1 can be written in terms of a trace of a fermion loop.

By definition, the hard-scattering amplitude T_H is free of collinear singularities and has a well-defined expansion in $\alpha_S(\mu_R^2)$ of the form

$$T_H(x,y,Q^2,\mu_R^2,\mu_F^2) = \alpha_S(\mu_R^2) T_H^{(0)}(x,y,Q^2) \Bigg[1 + \frac{\alpha_S(\mu_R^2)}{\pi} T_H^{(1)}(x,y,\mu_R^2/Q^2,\mu_F^2/Q^2) + \cdots \Bigg], \tag{2.1}$$

where

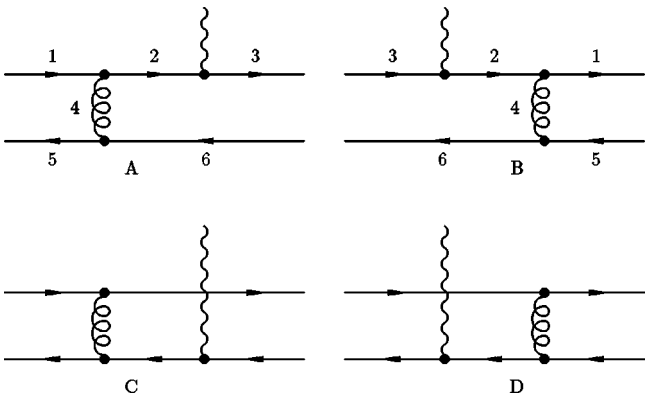

FIG. 2. Lowest-order Feynman diagrams contributing to the $(q_1\bar{q}_2)+\gamma^*\to(q_1\bar{q}_2)$ amplitude.

$$\alpha_S(\mu_R^2)=\frac{4\pi}{\beta_0\,\ln(\mu_R^2/\Lambda_{QCD}^2)}, \tag{2.2}$$

and

$$\beta_0=11-\frac{2}{3}n_f, \tag{2.3}$$

with n_f being the effective number of quark flavors and Λ_{QCD} is the fundamental QCD parameter.

In the LO approximation (Born approximation) there are only four Feynman diagrams contributing to the $(q_1\bar{q}_2)+\gamma^*\to(q_1\bar{q}_2)$ transition amplitude. They are shown in Fig. 2. Evaluating these diagrams, one finds that the LO hard-scattering amplitude is given by

$$T_H^{(0)}(x,y,Q^2)=\frac{4}{3}\frac{16\pi}{Q^2(1-x)(1-y)}. \tag{2.4}$$

To obtain this result, it is necessary to evaluate only one of the four diagrams. Namely, knowing the contribution of diagram *A*, the contribution of diagrams *B*, *C*, and *D* can be obtained by making use of the isospin symmetry and time-reversal symmetry. In the leading-twist approximation, the isospin symmetry is exact. A consequence of this is that the contributions of diagrams *A* and *B* are related to the contributions of *C* and *D*, respectively. On the other hand, diagrams *A* and *C* are by time-reversal symmetry related to diagrams *B* and *D*, respectively.

At NLO there are altogether 62 one-loop Feynman diagrams contributing to the $(q_1\bar{q}_2)+\gamma^*\to(q_1\bar{q}_2)$ amplitude. They can be generated by inserting an internal gluon line into the leading-order diagrams of Fig. 2. Use of the above mentioned symmetries (isospin and time-reversal) cuts the number of independent one-loop diagrams to be evaluated from 62 to 17. They are all generated from the LO diagram *A*. We use the notation where Aij is the diagram obtained from diagram *A* by inserting the gluon line connecting the lines i and j, where $i,j=1,2,\cdots,6$. They are shown in Fig. 3

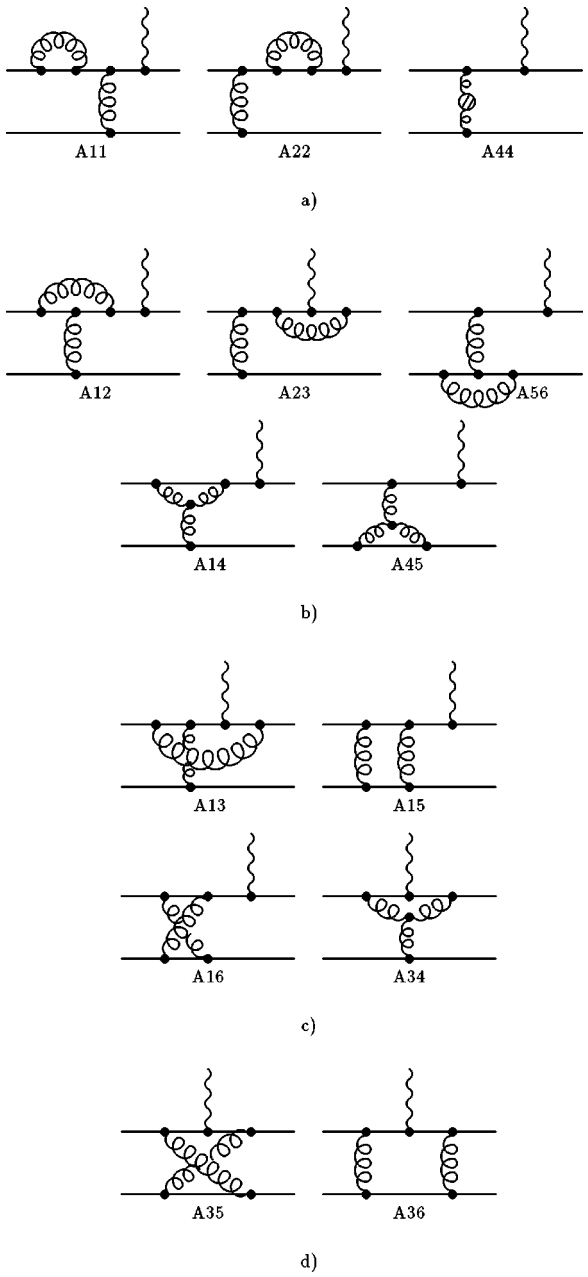

FIG. 3. Distinct one-loop Feynman diagrams contributing to the $(q_1\bar{q}_2)+\gamma^*\to(q_1\bar{q}_2)$ amplitude. The total number of diagrams is 62.

with the exception of $A33$, $A55$, and $A66$, which give obviously the same contribution as $A11$. These diagrams contain ultraviolet (UV) singularities and, owing to the fact that initial- and final-state quarks are massless and onshell, they also contain both infrared (IR) and collinear singularities. We use dimensional regularization in $D=4-2\epsilon$ dimensions to regularize all three types of singularities, distinguishing the poles $1/\epsilon$ by the subscripts UV and IR ($D=4-2\epsilon_{UV}$, $4+2\epsilon_{IR}$). Soft singularity is always accompanied by two collinear singularities and, consequently, when dimensionally regularized, leads to the double pole $1/\epsilon_{IR}^2$.

Before the subtraction of divergences has been performed,

TABLE I. Contributions to $\Delta^{(1)}(u,v,\mu_R^2/Q^2,\mu_F^2/Q^2)$ [defined by Eq. (2.6)] of Feynman diagrams shown in Fig. 3.

A11	$-\frac{1}{12}(\eta_{UV}+\eta_{IR})$
A22	$-\frac{1}{6}(\eta_{UV}-\ln\overline{v})$
A44	$\frac{1}{8}\left[\left(5-\frac{2}{3}n_f\right)(\eta_{UV}-\ln(\overline{uv}))+\frac{16}{3}-\frac{4}{9}n_f\right]$
A23	$\frac{1}{6}\left(\eta_{UV}+\frac{1+\overline{v}}{v}\ln\overline{v}\right)$
A12	$-\frac{1}{48}\left[\eta_{UV}+2\eta_{IR}\left(1+\frac{\overline{u}}{u}\ln\overline{u}\right)-3-\frac{\overline{u}}{u}\ln\overline{u}+\ln\overline{v}+\frac{\overline{u}}{u}\ln^2\overline{u}+2\frac{\overline{u}}{u}\ln\overline{u}\ln\overline{v}\right]$
A56	$-\frac{1}{48}[\eta_{UV}+2\eta_{IR}(1-\ln(\overline{uv}))-2\tilde{\eta}_{IR}-5+\ln(\overline{uv})-\ln^2\overline{u}-\ln^2\overline{v}-2\ln\overline{u}\ln\overline{v}]$
A14	$\frac{3}{16}\left[3\eta_{UV}+2\eta_{IR}\left(1+\frac{\ln\overline{u}}{u}\right)+1+\ln\frac{\overline{u}}{v}+\frac{\ln^2\overline{u}}{u}+2\frac{\ln\overline{u}\ln\overline{v}}{u}\right]$
A45	$\frac{3}{16}[3\eta_{UV}+4\eta_{IR}-1+\ln(\overline{uv})]$
A15	$-\frac{1}{3}\frac{\overline{u}}{u}\left[\eta_{IR}\ln\overline{u}+\ln\overline{u}+\frac{1}{2}\ln^2\overline{u}+\ln\overline{u}\ln\overline{v}\right]$
A16	$-\frac{1}{24}\left[\tilde{\eta}_{IR}+\eta_{IR}\left(1+\frac{\ln\overline{u}}{u}+2\ln u+\ln\overline{v}\right)+\frac{\ln\overline{u}}{u}+2\ln u+\ln\overline{v}+\frac{1}{2}\frac{\ln^2\overline{u}}{u}+\ln^2 u+\frac{1}{2}\ln^2\overline{v}+\frac{\ln\overline{u}\ln\overline{v}}{u}+2\ln u\ln\overline{v}\right]$
A34	$\frac{3}{8}\left[\eta_{IR}\left(2+\frac{\ln\overline{u}}{u}+\frac{\ln\overline{v}}{v}\right)-2+\ln\overline{u}+\ln\overline{v}+\frac{\overline{u}+\overline{v}}{uv}\ln\overline{u}\ln\overline{v}+\frac{1}{2u}\ln^2\overline{u}+\frac{1}{2v}\ln^2\overline{v}\right]$
A13	$\frac{1}{24}\left\{\tilde{\eta}_{IR}+\eta_{IR}\left(\frac{\overline{u}}{u}\ln\overline{u}+\ln u+\ln v\right)+1+\frac{\overline{u}}{2u}\ln^2\overline{u}+\frac{1}{2}\ln^2 u+\frac{1}{2}\ln^2 v+\ln u\ln v+\frac{\overline{u}}{u}\ln\overline{u}\ln\overline{v}-\frac{1}{2(u-v)^2}\left[4\overline{u}^2u\mathrm{H}(u,\overline{v})+(4u-5u^2+v^2)(\ln u+\ln v)+(6u-5u^2-2v+v^2)u\frac{\ln\overline{u}}{u}+(2u-4u^2+2v-4uv+5u^2v-v^3)\frac{\ln\overline{v}}{v}\right]\right\}$
A36	$-\frac{1}{3}\left[\eta_{IR}\left(\frac{\overline{u}}{u}\ln\overline{u}+\frac{\overline{v}}{v}\ln\overline{v}\right)+\frac{\overline{u}}{u}\ln\overline{u}+\frac{\overline{v}}{v}\ln\overline{v}+\frac{\overline{u}}{2u}\ln^2\overline{u}+\frac{\overline{v}}{2v}\ln^2\overline{v}+\frac{\overline{u}+\overline{v}}{uv}\ln\overline{u}\ln\overline{v}\right]$
A35	$-\frac{1}{24}\left[2\tilde{\eta}_{IR}+\eta_{IR}\left(2+\frac{1+u}{u}\ln\overline{u}+\frac{1+v}{v}\ln\overline{v}\right)-2(1-u-v)\mathrm{H}(u,v)+\frac{1+u}{u}\ln\overline{u}+\frac{1+v}{v}\ln\overline{v}+\frac{1+u}{2u}\ln^2\overline{u}+\frac{1+v}{2v}\ln^2\overline{v}+\frac{\overline{u}+\overline{v}}{uv}\ln\overline{u}\ln\overline{v}\right]$

the pion form factor convolution formula reads

$$F_\pi(Q^2)=\int_0^1 du\int_0^1 dv \times\Phi^*(v)\Delta(u,v,\mu_{UV}^2/Q^2,\mu_{IR}^2/Q^2)\Phi(u), \quad (2.5)$$

where $\Delta(u,v,\mu_{UV}^2/Q^2,\mu_{IR}^2/Q^2)$ denotes the amplitude for the $(q_1\bar{q}_2)+\gamma^*\to(q_1\bar{q}_2)$ quark subprocess. This amplitude has the expansion of the form

$$\Delta(u,v,\mu_{UV}^2/Q^2,\mu_{IR}^2/Q^2)=\alpha_S\Delta^{(0)}(u,v,Q^2) + \frac{\alpha_S^2}{\pi}\Delta^{(1)}(u,v,\mu_{UV}^2/Q^2,\mu_{IR}^2/Q^2) + \ldots, \quad (2.6)$$

where

$$\Delta^{(0)}(u,v,Q^2)=(1-\epsilon)T_H^{(0)}(u,v,Q^2). \quad (2.7)$$

The contributions of the individual diagrams to $\Delta^{(1)}(u,v,\mu_{UV}^2/Q^2,\mu_{IR}^2/Q^2)$, with the overall factor $T_H^{(0)}(u,v,Q^2)$ of Eq. (2.4) extracted, are listed in Table I. We have used the following notation:

$$\bar{u}=1-u,\quad \bar{v}=1-v,$$

$$\eta_{UV}=\frac{1}{\epsilon_{UV}}-\gamma-\ln\frac{Q^2}{4\pi\mu_{UV}^2}=\frac{1}{\hat{\epsilon}_{UV}}+\ln\frac{\mu_{UV}^2}{Q^2},$$

$$\eta_{IR}=\frac{1}{\epsilon_{IR}}+\gamma+\ln\frac{Q^2}{4\pi\mu_{IR}^2}=\frac{1}{\hat{\epsilon}_{IR}}-\ln\frac{\mu_{IR}^2}{Q^2},$$

$$\tilde{\eta}_{IR}=\frac{1}{\epsilon_{IR}^2}+\frac{1}{\epsilon_{IR}}\left(\gamma+\ln\frac{Q^2}{4\pi\mu_{IR}^2}\right)+\frac{1}{2}\left(\gamma^2-\frac{\pi^2}{6}\right) +\gamma\ln\frac{Q^2}{4\pi\mu_{IR}^2}+\frac{1}{2}\ln^2\frac{Q^2}{4\pi\mu_{IR}^2},$$

$$\frac{1}{\hat{\epsilon}_{UV}}=\frac{1}{\epsilon_{UV}}-\gamma+\ln(4\pi),$$

$$\frac{1}{\hat{\epsilon}_{IR}}=\frac{1}{\epsilon_{IR}}+\gamma-\ln(4\pi). \quad (2.8)$$

The function $\mathrm{H}(u,v)$ appearing in Table I is given by the expression

$$\mathrm{H}(u,v)=\frac{1}{1-u-v}\left[\mathrm{Li}_2\left(\frac{\bar{v}}{u}\right)+\mathrm{Li}_2\left(\frac{\bar{u}}{v}\right)+\mathrm{Li}_2\left(\frac{uv}{\bar{u}\bar{v}}\right) -\mathrm{Li}_2\left(\frac{u}{\bar{v}}\right)-\mathrm{Li}_2\left(\frac{v}{\bar{u}}\right)-\mathrm{Li}_2\left(\frac{\bar{u}\bar{v}}{uv}\right)\right], \quad (2.9)$$

where $\mathrm{Li}_2(u)$ is the Spence function defined as

$$\mathrm{Li}_2(u)=-\int_0^u\frac{\ln(1-t)}{t}dt. \quad (2.10)$$

Adding up the contributions of all diagrams, we find that the NLO contribution to the $(q_1\bar{q}_2)+\gamma^*\to(q_1\bar{q}_2)$ amplitude, given in Eq. (2.6), can be written in the form

$$\Delta^{(1)}(u,v,\mu_{UV}^2/Q^2,\mu_{IR}^2/Q^2) =T_H^{(0)}(u,v,Q^2)\left[C_{UV}\frac{1}{\hat{\epsilon}_{UV}}+C_{IR}(u,v)\frac{1}{\hat{\epsilon}_{IR}} +\tilde{f}_{UV}(u,v,\mu_{UV}^2/Q^2)+\tilde{f}_{IR}(u,v,\mu_{IR}^2/Q^2)+\tilde{f}_C(u,v)\right], \quad (2.11)$$

where

$$C_{UV}=\frac{1}{4}\beta_0, \quad (2.12a)$$

$$C_{IR}(u,v)=\frac{2}{3}[3+\ln(\bar{u}\bar{v})], \quad (2.12b)$$

and

$$\tilde{f}_{UV}(u,v,\mu_{UV}^2/Q^2)=C_{UV}\left[\frac{2}{3}-\ln(\bar{u}\bar{v})+\ln\frac{\mu_{UV}^2}{Q^2}\right], \quad (2.13a)$$

$$\tilde{f}_{IR}(u,v,\mu_{IR}^2/Q^2)=C_{IR}(u,v)\left[\frac{1}{2}\ln(\bar{u}\bar{v})-\ln\frac{\mu_{IR}^2}{Q^2}\right], \quad (2.13b)$$

$$\tilde{f}_C(u,v)=\frac{1}{12}[-10+20\ln(\bar{u}\bar{v})+\ln u\ln v +\ln\bar{u}\ln\bar{v}-\ln u\ln\bar{v}-\ln\bar{u}\ln v +(1-u-v)\mathrm{H}(u,v)+\mathrm{R}(u,v)]. \quad (2.13c)$$

The function $\mathrm{R}(u,v)$ is defined as

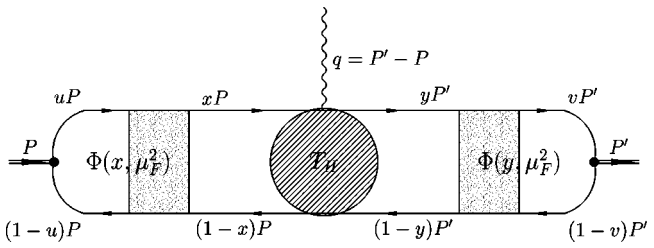

FIG. 4. Pictorial representation of the procedure for absorbing the collinear divergences into the pion distribution amplitude $\Phi(x,\mu_F^2)$.

$$\mathrm{R}(u,v)=\frac{1}{(u-v)^2}\Bigg[(2uv-u-v)(\ln u+\ln v) +(-2uv^2-2v^2+10uv-2v-4u^2)\frac{\ln \bar{v}}{v} +(-2vu^2-2u^2+10uv-2u-4v^2)\frac{\ln \bar{u}}{u} -(v\bar{v}^2+u\bar{u}^2)\mathrm{H}(u,\bar{v})\Bigg]. \tag{2.14}$$

The contributions of the individual diagrams listed in Table I are in agreement with those obtained in Ref. [5] (up to some typographical errors listed in [9]). Correspondence between our results and those of Ref. [5] is established by multiplying the latter by $(P+P')^\mu/Q^2$.

It is easily seen from Eqs. (2.11)–(2.14) that in summing up the contributions of all diagrams to the exclusive $(q_1\bar{q}_2)+\gamma^*\to(q_1\bar{q}_2)$ amplitude, the originally present soft singularities (double $1/\epsilon_{IR}^2$ poles) cancel out, as required. The final result for the amplitude contains $1/\epsilon_{UV}$ and only simple $1/\epsilon_{IR}$ poles.

We now proceed to treat these poles. When doing this, one has to exercise some care, since the subtractions have to be performed in such a way that the universality of the distribution amplitude as well as the universality of the coupling constant are simultaneously preserved.

The IR poles in Eq. (2.11), related to collinear singularities, are such that they can be absorbed into the pion distribution amplitude. The universality of the distribution amplitude requires that the poles $1/\epsilon_{IR}$ should be absorbed by some universal renormalization factor [8,21]. The regularization-dependent terms represent ''soft'' effects and therefore we absorb them into the distribution amplitude along with the singularities. A crucial observation is that the structure of the collinearly divergent terms in Eq. (2.11) is such that one can write

$$V_1(v,y)\otimes T_H^{(0)}(x,y,Q^2)\otimes\delta(x-u) +\delta(v-y)\otimes T_H^{(0)}(x,y,Q^2)\otimes V_1(x,u) =C_{IR}(u,v)T_H^{(0)}(u,v,Q^2), \tag{2.15}$$

where the function $V_1(x,u)$ is the one-loop evolution kernel for the pion distribution amplitude (see the corresponding expression in, for example, [5] or [22]), while $\otimes$ denotes the convolution symbol defined as

$$A(z)\otimes B(z)=\int_0^1 dz A(z)B(z). \tag{2.16}$$

Based on Eq. (2.15), the NLO expression for the $(q_1\bar{q}_2)+\gamma^*\to(q_1\bar{q}_2)$ amplitude, given by Eqs. (2.6), (2.11)–(2.14), can be written in a factorized form

$$\alpha_S\Delta^{(0)}(u,v,Q^2;\epsilon_{IR})+\frac{\alpha_S^2}{\pi}\Delta^{(1)}(u,v,\mu_{IR}^2/Q^2;1/\epsilon_{IR}) =\left[\delta(v-y)+\frac{\alpha_S}{\pi}V_1(v,y)\left(\frac{1}{\hat{\epsilon}_{IR}}+\ln\frac{\mu_F^2}{\mu_{IR}^2}\right)\right] \otimes\left\{\alpha_S T_H^{(0)}(x,y,Q^2)\left[(1-\epsilon) +\frac{\alpha_S}{\pi}\hat{T}_H^{(1)}(x,y,\mu_F^2/Q^2;\epsilon_{IR})\right]\right\} \otimes\left[\delta(x-u)+\frac{\alpha_S}{\pi}V_1(x,u)\left(\frac{1}{\hat{\epsilon}_{IR}}+\ln\frac{\mu_F^2}{\mu_{IR}^2}\right)\right]. \tag{2.17}$$

Formula (2.17) shows the essence of the procedure for the separation of collinear divergences, which is schematically represented in Fig. 4. The procedure consists of summing the effects of collinear divergences contained in the shaded rectangular region in Fig. 4, as a result of which the outside quark (antiquark) with momentum uP $(\bar{u}P)$ ends up on the inside quark (antiquark) of momentum xP $(\bar{x}P)$.

As for the UV poles, we renormalize them using the modified minimal-subtraction scheme. This is carried out by stating that α_S appearing in Eq. (2.6) is the bare unrenormalized coupling related to the renormalized physical coupling $\alpha_{\overline{\mathrm{MS}}}(\mu_R^2)$ by

$$\alpha_S=\alpha_{\overline{\mathrm{MS}}}(\mu_R^2)\left[1-\frac{\alpha_{\overline{\mathrm{MS}}}(\mu_R^2)}{\pi}\frac{\beta_0}{4}\left(\frac{1}{\hat{\epsilon}_{UV}}-\ln\frac{\mu_R^2}{\mu_{UV}^2}\right)\right]. \tag{2.18}$$

It is important to note that the $\epsilon\to 0$ limit can be taken only after the separation of collinear divergences and UV renormalization have been performed [taking the $\epsilon\to 0$ limit in $\Delta^{(0)}$ before the subtraction of IR and UV singularities is equivalent to choosing a factorization scheme that does not respect the universality of the distribution amplitude (see [8]) and the renormalization scheme in which the running coupling constant is not universal]. As a result, we obtain the following expression for the NLO hard-scattering amplitude for the pion form factor:

$$T_H(x,y,Q^2,\mu_R^2,\mu_F^2) = \alpha_{\overline{\rm MS}}(\mu_R^2)T_H^{(0)}(x,y,Q^2) \times\left[1+\frac{\alpha_{\overline{\rm MS}}(\mu_R^2)}{\pi}T_H^{(1)}(x,y,\mu_R^2/Q^2,\mu_F^2/Q^2)\right], \quad (2.19)$$

where

$$T_H^{(1)}(x,y,\mu_R^2/Q^2,\mu_F^2/Q^2) = f_{UV}(x,y,\mu_R^2/Q^2)+f_{IR}(x,y,\mu_F^2/Q^2)+f_C(x,y), \quad (2.20)$$

and

$$f_{UV}(x,y,\mu_R^2/Q^2)=\tilde{f}_{UV}(x,y,\mu_R^2/Q^2)+C_{UV} =\frac{1}{4}\beta_0\left[\frac{5}{3}-\ln(\overline{xy})+\ln\frac{\mu_R^2}{Q^2}\right], \quad (2.21a)$$

$$f_{IR}(x,y,\mu_F^2/Q^2)=\tilde{f}_{IR}(x,y,\mu_F^2/Q^2) =\frac{2}{3}[3+\ln(\overline{xy})]\left[\frac{1}{2}\ln(\overline{xy})-\ln\frac{\mu_F^2}{Q^2}\right], \quad (2.21b)$$

$$f_C(x,y)=\tilde{f}_C(x,y)-C_{IR}(x,y) =\frac{1}{12}[-34+12\ln(\overline{xy})+\ln x\ln y +\ln\overline{x}\ln\overline{y}-\ln x\ln\overline{y}-\ln\overline{x}\ln y +(1-x-y)\mathrm{H}(x,y)+\mathrm{R}(x,y)]. \quad (2.21c)$$

A few comments on the previously performed calculations are in order. Our final expression for the hard-scattering amplitude T_H is in agreement with Ref. [7]. The calculation of [5] contains a few typographical errors in the diagram-by-diagram listing as well as in the final expression (which are all listed in [9]). Apart from this, the results from Ref. [5] agree with ours. In Refs. [6,8] the contribution of the diagrams with propagator corrections on external quark lines were not taken into account. Also, in Ref. [6] the subtraction of collinear singularities was performed in a way that is not consistent with the universality of the distribution amplitude (see the discussion in Ref. [8]). Finally, a thorough analysis of the results of Refs. [5–7] was performed in Ref. [9], but in obtaining the final expression for the hard-scattering amplitude T_H, collinear and UV divergences were subtracted in a way that is not consistent with the universality of both the distribution amplitude and the running coupling constant.

III. EVOLUTIONAL CORRECTIONS TO THE PION DISTRIBUTION AMPLITUDE

The pion distribution amplitude $\Phi(x,\mu_F^2)$, controlling exclusive pion processes at large momentum transfer, is the basic valence wave function of the pion. Its form is not yet accurately known. It has been shown, however, that the leptonic decay $\pi^+\to\mu^+\nu_\mu$ imposes on $\Phi(x,\mu_F^2)$ a constraint of the form

$$\int_0^1 dx\ \Phi(x,\mu_F^2)=\frac{f_\pi}{2\sqrt{2n_C}}. \quad (3.1)$$

Given the form of $\Phi(x,\mu_F^2)$, this relation normalizes it for any μ_F^2. In Eq. (3.1), $f_\pi=0.131$ GeV is the pion decay constant and $n_C(=3)$ is the number of QCD colors.

Instead of using $\Phi(x,\mu_F^2)$ satisfying Eq. (3.1), one usually introduces the distribution amplitude $\phi(x,\mu_F^2)$ normalized to unity,

$$\int_0^1 dx\ \phi(x,\mu_F^2)=1, \quad (3.2)$$

and related to $\Phi(x,\mu_F^2)$ by

$$\Phi(x,\mu_F^2)=\frac{f_\pi}{2\sqrt{2n_C}}\phi(x,\mu_F^2). \quad (3.3)$$

Although intrinsically nonperturbative, the pion distribution amplitude $\phi(x,\mu_F^2)$ satisfies an evolution equation of the form

$$\mu_F^2\frac{\partial}{\partial\mu_F^2}\phi(x,\mu_F^2)=\int_0^1 du\ \ V(x,u,\alpha_S(\mu_F^2))\ \ \phi(u,\mu_F^2), \quad (3.4)$$

in which the evolution kernel is calculable in perturbation theory:

$$V(x,u,\alpha_S(\mu_F^2))=\frac{\alpha_S(\mu_F^2)}{\pi}V_1(x,u)+\left(\frac{\alpha_S(\mu_F^2)}{\pi}\right)^2 V_2(x,u)+\cdots \quad (3.5)$$

and has been computed in the one- and two-loop approximations using dimensional regularization and the $\overline{\rm MS}$ scheme.

If the distribution amplitude $\phi(x,\mu_0^2)$ can be calculated at an initial momentum scale μ_0^2 using QCD sum rules [23] or lattice gauge theory [24], then the differential-integral evolution equation (3.4) can be integrated using the moment method to give $\phi(x,\mu_F^2)$ at any momentum scale $\mu_F^2>\mu_0^2$.

Because of the complicated structure of the two-loop contribution to the evolutional kernel $V_2(x,y)$, only the first few moments of the evolutional kernel have been computed numerically.

Recently, based on the conformal spin expansion and the conformal consistency relation, the analytical result for the evolution of the flavor-nonsinglet meson distribution amplitude has been determined [20].

To the NLO approximation, this rather complicated solution has the form

$$\phi(x,\mu_F^2)=\phi^{LO}(x,\mu_F^2)+\frac{\alpha_S(\mu_F^2)}{\pi}\phi^{NLO}(x,\mu_F^2), \tag{3.6}$$

where

$$\phi^{LO}(x,\mu_F^2)=x(1-x)\sum_{n=0}^{\infty}{}' \; C_n^{3/2}(2x-1)\;\frac{4(2n+3)}{(n+1)(n+2)}\left(\frac{\alpha_S(\mu_0^2)}{\alpha_S(\mu_F^2)}\right)^{\gamma_n^{(0)}/\beta_0}\int_0^1 dy C_n^{3/2}(2y-1)\,\phi(y,\mu_0^2), \tag{3.7}$$

and

$$\begin{aligned}\phi^{NLO}(x,\mu_F^2)=x(1-x)\sum_{n=0}^{\infty}{}' &\left(\frac{\alpha_S(\mu_0^2)}{\alpha_S(\mu_F^2)}\right)^{\gamma_n^{(0)}/\beta_0}\int_0^1 dy C_n^{3/2}(2y-1)\,\phi(y,\mu_0^2)\\ &\times\left[C_n^{3/2}(2x-1)\frac{(2n+3)}{(n+1)(n+2)}\left(1-\frac{\alpha_S(\mu_0^2)}{\alpha_S(\mu_F^2)}\right)\left(\frac{\gamma_n^{(1)}}{2\beta_0}+\frac{\beta_1}{\beta_0^2}\gamma_n^{(0)}\right)\right.\\ &\left.+\sum_{k=n+2}^{\infty}{}' \;\; C_k^{3/2}(2x-1)\frac{2(2k+3)}{(k+1)(k+2)}S_{kn}(\mu_F^2)C_{kn}^{(1)}\right],\end{aligned} \tag{3.8}$$

with abbreviations

$$S_{kn}(\mu_F^2)=\frac{\gamma_k^{(0)}-\gamma_n^{(0)}}{\gamma_k^{(0)}-\gamma_n^{(0)}+\beta_0}\left[1-\left(\frac{\alpha_S(\mu_0^2)}{\alpha_S(\mu_F^2)}\right)^{1+(\gamma_k^{(0)}-\gamma_n^{(0)})/\beta_0}\right], \tag{3.9}$$

$$C_{kn}^{(1)}=(2n+3)\left[\frac{\gamma_n^{(0)}-\beta_0+4C_FA_{kn}}{(k-n)(k+n+3)}+\frac{2C_F(A_{kn}-\psi(k+2)+\psi(1))}{(n+1)(n+2)}\right], \tag{3.10}$$

$$A_{kn}=\psi\left(\frac{k+n+4}{2}\right)-\psi\left(\frac{k-n}{2}\right)+2\psi(k-n)-\psi(k+2)-\psi(1), \tag{3.11}$$

and Σ' denoting the sum running only over even n, while $C_n^{3/2}(z)$ are Gegenbauer polynomials of order 3/2 and $C_F=4/3$. In Eqs. (3.7)–(3.10), $\gamma_n^{(0)}$ are the usual anomalous dimensions:

$$\gamma_n^{(0)}=C_F\left[3+\frac{2}{(n+1)(n+2)}-4\sum_{i=1}^{n+1}\frac{1}{i}\right], \tag{3.12}$$

while β_0 and β_1 are the first two terms in the expansion of the QCD β-function, with β_0 given by Eq. (2.3), and

$$\beta_1=102-\frac{38}{3}n_f. \tag{3.13}$$

The function $\psi(z)$ appearing in Eqs. (3.10) and (3.11) is defined as

$$\psi(z)=\frac{d}{dz}(\ln\Gamma(z)). \tag{3.14}$$

For $n_f=3$ and for the values of n we are interested in, we have taken the values of the anomalous dimension $\gamma_n^{(1)}$ from [25,26]:

$$\gamma_0^{(1)}=0, \quad \gamma_2^{(1)}=111.03, \quad \gamma_4^{(1)}=150.28. \tag{3.15}$$

To proceed, we expand the distribution amplitude $\phi(x,\mu_0^2)$ in terms of the Gegenbauer polynomials $C_n^{3/2}(2x-1)$ (the eigenfunctions of the LO evolution equation):

$$\phi(x)=\phi(x,\mu_0^2)=6x(1-x)\sum_{n=0}^{\infty}{}' B_n C_n^{3/2}(2x-1). \tag{3.16}$$

Owing to the orthogonality of the Gegenbauer polynomials, the expansion coefficients B_n are given by

$$B_n=\frac{1}{6}\frac{4(2n+3)}{(n+1)(n+2)}\int_0^1 dx C_n^{3/2}(2x-1)\phi(x) \tag{3.17}$$

and the normalization condition (3.2) then implies $B_0=1$. Substituting Eq. (3.16) into Eq. (3.7) gives

$$\phi^{LO}(x,\mu_F^2)=6x(1-x)\sum_{n=0}^{\infty}{}' B_n^{LO}(\mu_F^2)\ \ C_n^{3/2}(2x-1), \tag{3.18}$$

where

$$B_n^{LO}(\mu_F^2)=B_n\left(\frac{\alpha_S(\mu_0^2)}{\alpha_S(\mu_F^2)}\right)^{\gamma_n^{(0)}/\beta_0}, \tag{3.19}$$

so that, obviously, $B_0^{LO}=1$. Next, by taking Eq. (3.16) into account Eq. (3.8) becomes

$$\phi^{NLO}(x,\mu_F^2)=6x(1-x)\sum_{k=2}^{\infty}{}' B_k^{NLO}(\mu_F^2)C_k^{3/2}(2x-1), \tag{3.20}$$

where

$$B_k^{NLO}(\mu_F^2)=B_k^{LO}(\mu_F^2)P_k(\mu_F^2)+\sum_{n=0}^{k-2}{}' B_n^{LO}(\mu_F^2)Q_{kn}(\mu_F^2), \tag{3.21}$$

and

$$P_k(\mu_F^2)=\frac{1}{4}\left(\frac{\gamma_k^{(1)}}{2\beta_0}+\frac{\beta_1}{\beta_0^2}\gamma_k^{(0)}\right)\left(1-\frac{\alpha_S(\mu_0^2)}{\alpha_S(\mu_F^2)}\right), \tag{3.22}$$

$$Q_{kn}(\mu_F^2)=\frac{(2k+3)}{(k+1)(k+2)}\times\frac{(n+2)(n+1)}{2(2n+3)}C_{kn}^{(1)}S_{kn}(\mu_F^2). \tag{3.23}$$

For the purpose of our calculation, we use the following four candidate distribution amplitudes (shown in Fig. 5) as nonperturbative inputs at the reference momentum scale $\mu_0^2=(0.5\ \text{GeV})^2$:

$$\phi_{as}(x)\equiv\phi_{as}(x,\mu_0^2)=6x(1-x), \tag{3.24a}$$

$$\phi_{CZ}(x)\equiv\phi_{CZ}(x,\mu_0^2)=6x(1-x)[5(2x-1)^2], \tag{3.24b}$$

$$\phi_{P2}(x)\equiv\phi_{P2}(x,\mu_0^2)=6x(1-x)[-0.1821+5.91(2x-1)^2], \tag{3.24c}$$

$$\phi_{P3}(x)\equiv\phi_{P3}(x,\mu_0^2)=6x(1-x)[0.6016-4.659(2x-1)^2+15.52(2x-1)^4]. \tag{3.24d}$$

Here $\phi_{as}(x)$ is the asymptotic distribution amplitude and represents the solution of the evolution equation (3.4) for $\mu_F^2\to\infty$. The double-hump-shaped distribution amplitudes $\phi_{CZ}(x)$ and $\phi_{P2}(x)$ and the three-hump-shaped distribution amplitude $\phi_{P3}(x)$ have been obtained using the method of QCD sum rules [23,27]. As Fig. 5 shows, these distribution amplitudes, unlike $\phi_{as}(x)$, are strongly end-point concentrated. In the limit $\mu_F^2\to\infty$, they reduce to the asymptotic form $\phi_{as}(x)$.

The pion candidate distribution amplitudes given by Eq. (3.24) are of the general form

$$\phi(x)=\phi(x,\mu_0^2)=\phi_{as}(x)[1+B_2C_2^{3/2}(2x-1)+B_4C_4^{3/2}(2x-1)], \tag{3.25}$$

with the corresponding coefficients

$$\phi_{as}(x):\quad B_n=0,\ \ n\geqslant 2 \tag{3.26a}$$

$$\phi_{CZ}(x):\quad B_n=0,\ \ n>2\quad B_2=2/3 \tag{3.26b}$$

$$\phi_{P2}(x):\quad B_n=0,\ \ n>2\quad B_2=0.788 \tag{3.26c}$$

$$\phi_{P3}(x):\quad B_n=0,\ \ n>4\quad B_2=0.7582\quad B_4=0.3941, \tag{3.26d}$$

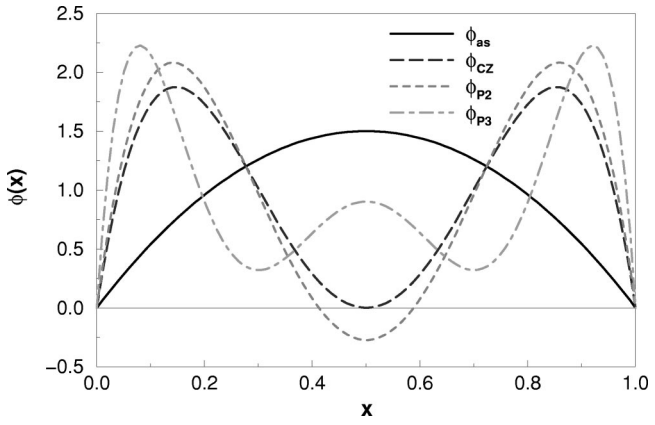

FIG. 5. The four candidate pion distribution amplitudes defined by Eq. (3.24), chosen as nonperturbative inputs at the reference scale $\mu_0^2=(0.5\ \text{GeV})^2$.

with $B_0=1$. Now, according to Eqs. (3.18) and (3.20), the LO and NLO parts of the distribution amplitude (3.25) read

$$\phi^{LO}(x,\mu_F^2)=\phi_{as}(x)[1+B_2^{LO}(\mu_F^2)C_2^{3/2}(2x-1) + B_4^{LO}(\mu_F^2)C_4^{3/2}(2x-1)], \tag{3.27}$$

$$\phi^{NLO}(x,\mu_F^2)=\phi_{as}(x)\Bigg[B_2^{NLO}(\mu_F^2)C_2^{3/2}(2x-1) + B_4^{NLO}(\mu_F^2)C_4^{3/2}(2x-1) + {\sum_{k=6}^{\infty}}' B_k^{NLO}(\mu_F^2)C_k^{3/2}(2x-1)\Bigg], \tag{3.28}$$

where

$$B_2^{LO}(\mu_F^2)=B_2\left(\frac{\alpha_S(\mu_0^2)}{\alpha_S(\mu_F^2)}\right)^{-50/81},$$

$$B_4^{LO}(\mu_F^2)=B_4\left(\frac{\alpha_S(\mu_0^2)}{\alpha_S(\mu_F^2)}\right)^{-364/405}, \tag{3.29}$$

and

$$B_2^{NLO}(\mu_F^2)=B_2^{LO}(\mu_F^2)P_2(\mu_F^2)+Q_{20}(\mu_F^2),$$

$$B_4^{NLO}(\mu_F^2)=B_4^{LO}(\mu_F^2)P_4(\mu_F^2)+Q_{40}(\mu_F^2) + B_2^{LO}(\mu_F^2)Q_{42}(\mu_F^2),$$

$$B_k^{NLO}(\mu_F^2)=Q_{k0}(\mu_F^2)+B_2^{LO}(\mu_F^2)Q_{k2}(\mu_F^2) + B_4^{LO}(\mu_F^2)Q_{k4}(\mu_F^2),\quad k\geqslant 6. \tag{3.30}$$

Note that $\phi^{NLO}(x,\mu_F^2)$ represents the infinite sum of Gegenbauer polynomials even though the $\phi(x)$ distribution is described by a finite number of terms. Since B_k^{NLO} decreases with k, for the purpose of numerical calculation one can approximate $\phi^{NLO}(x,\mu_F^2)$ by neglecting higher-order Gegenbauer polynomials ($k>100$).

A summary of our results for the four candidate distribution amplitudes with the NLO evolutional corrections included is shown in Fig. 6. The dash-dotted curves correspond to the distribution amplitudes at the reference point $\mu_F^2=\mu_0^2=(0.5\ \text{GeV})^2$. The dashed and solid curves represent the distribution amplitudes evoluted to $\mu_F^2=(2\ \text{GeV})^2$, with the difference that the former includes only LO evolutional corrections, whereas the latter includes NLO evolutional corrections. As it is obvious from Eqs. (3.26a), (3.27), and (3.28), although ϕ_{as} shows no LO evolution, there are tiny effects of the NLO evolution. For other distributions, the LO evolution is significant, and even the NLO evolution is nonnegligible. Any distribution amplitude evolves asymptotically (i.e., for $\mu_F^2\to\infty$) into $\phi_{as}(x)$, but the higher μ_F^2 is, the ''slower'' this approach becomes.

IV. CHOOSING THE FACTORIZATION AND THE RENORMALIZATION SCALES

In this section we discuss various possibilities of choosing the renormalization scale μ_R and the factorization scale μ_F appropriate for the process under consideration.

Before starting the discussion, let us now, with the help of Eqs. (1.1), (2.1), and (3.6), write down the complete leading-twist NLO QCD expression for the pion electromagnetic form factor with the μ_R and μ_F dependence of all the terms explicitly indicated.

Generally, for the NLO form factor we can write

$$F_\pi(Q^2,\mu_R^2,\mu_F^2)=F_\pi^{(0)}(Q^2,\mu_R^2,\mu_F^2)+F_\pi^{(1)}(Q^2,\mu_R^2,\mu_F^2). \tag{4.1}$$

The first term in Eq. (4.1) is the LO contribution and is given by

$$F_\pi^{(0)}(Q^2,\mu_R^2,\mu_F^2)=\int_0^1 dx\int_0^1 dy\ \alpha_S(\mu_R^2) \times\Phi^{LO*}(y,\mu_F^2)T_H^{(0)}(x,y,Q^2)\Phi^{LO}(x,\mu_F^2). \tag{4.2}$$

The second term in Eq. (4.1) is the NLO contribution and can be written as

$$F_\pi^{(1)}(Q^2,\mu_R^2,\mu_F^2)=F_\pi^{(1a)}(Q^2,\mu_R^2,\mu_F^2)+F_\pi^{(1b)}(Q^2,\mu_R^2,\mu_F^2), \tag{4.3}$$

where

$$F_\pi^{(1a)}(Q^2,\mu_R^2,\mu_F^2) =\int_0^1 dx\int_0^1 dy\ \frac{\alpha_S^2(\mu_R^2)}{\pi}\ \Phi^{LO*}(y,\mu_F^2) \times T_H^{(0)}(x,y,Q^2)T_H^{(1)}(x,y,\mu_R^2/Q^2,\mu_F^2/Q^2) \times\Phi^{LO}(x,\mu_F^2) \tag{4.4}$$

is the contribution coming from the NLO correction to the hard-scattering amplitude, whereas

$$F_\pi^{(1b)}(Q^2,\mu_R^2,\mu_F^2) =\int_0^1 dx\int_0^1 dy\ \ \frac{\alpha_S(\mu_R^2)\alpha_S(\mu_F^2)}{\pi} \times[\Phi^{NLO*}(y,\mu_F^2)T_H^{(0)}(x,y,Q^2)\Phi^{LO}(x,\mu_F^2) + \Phi^{LO*}(y,\mu_F^2)T_H^{(0)}(x,y,Q^2)\Phi^{NLO}(x,\mu_F^2)] \tag{4.5}$$

is the contribution arising from the inclusion of the NLO evolution of the distribution amplitude. Now, if Eq. (2.4) is taken into account, the expression for the LO contribution of Eq. (4.2) can be written in the form

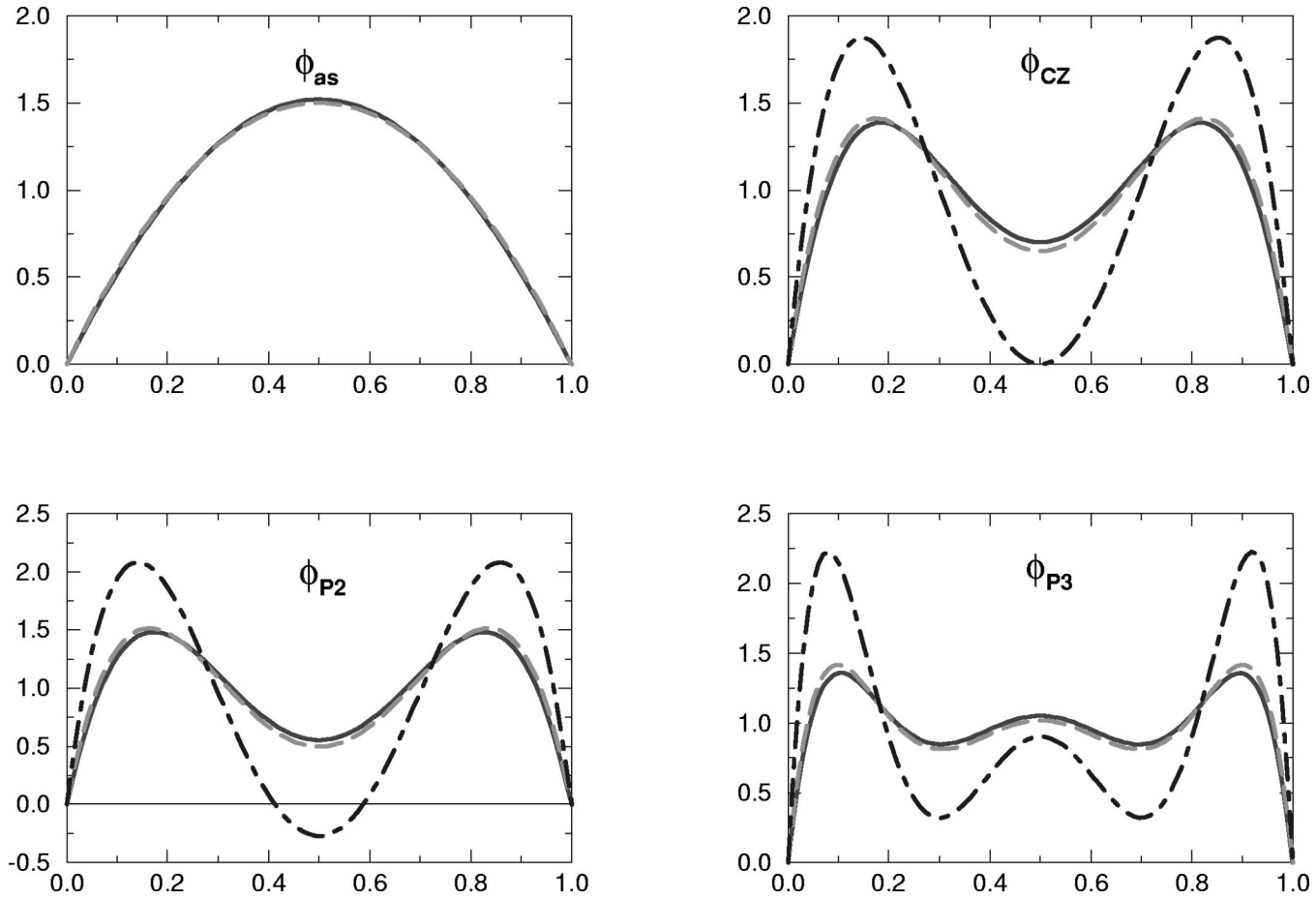

FIG. 6. Evolution of the four candidate pion distribution amplitudes: $\phi_{as}(x,\mu_F^2)$, $\phi_{CZ}(x,\mu_F^2)$, $\phi_{P2}(x,\mu_F^2)$, and $\phi_{P3}(x,\mu_F^2)$, with the running coupling constant $\alpha_S(\mu_F^2)$ and three active flavors. The dash-dotted curves correspond to the distribution amplitudes given by Eq. (3.24) and taken as nonperturbative input at the reference momentum scale $\mu_0^2=(0.5\ \text{GeV})^2$. The dashed curves correspond to the distribution amplitudes at the momentum scale $\mu_F^2=(2\ \text{GeV})^2$ with the LO evolutional corrections included according to (3.27). The solid curves correspond to the distribution amplitudes at the momentum scale $\mu_F^2=(2\ \text{GeV})^2$ with the NLO evolutional corrections taken into account according to Eqs. (3.6), (3.27) and (3.28).

$$F_\pi^{(0)}(Q^2,\mu_R^2,\mu_F^2)=\frac{8}{9}\pi\frac{f_\pi^2}{Q^2}\int_0^1 dx\int_0^1 dy\,\alpha_S(\mu_R^2) \times\frac{\phi^{LO}(x,\mu_F^2)}{\overline{x}}\ \frac{\phi^{LO*}(y,\mu_F^2)}{\overline{y}}. \tag{4.6}$$

Next, before going on to perform the remaining x and y integrations, we have to choose the renormalization scale μ_R and the factorization scale μ_F. In doing this, however, there is considerable freedom involved.

If calculated to all orders in perturbation theory, the physical pion form factor $F_\pi(Q^2)$, represented at the sufficiently high Q^2 by the factorization formula (1.1), would be independent of the renormalization and factorization scales, μ_R and μ_F, and so they are arbitrary parameters. Truncation of the perturbative expansion of $F_\pi(Q^2)$ at any finite order causes a residual dependence on these scales. Although the best choice for these scales remains an open question (the scale ambiguity problem), one would like to choose them in such a way that they are of an order of some physical scale in the problem, and, at the same time, to reduce the size of higher-order corrections as much as possible. Choosing any specific value for these scales leads to a theoretical uncertainty of the perturbative result.

In our calculation we approximate $F_\pi(Q^2)$ only by two terms of the perturbative series and hope that we can minimize higher-order corrections by a suitable choice of μ_R and μ_F, so that the LO term $F_\pi^{(0)}(Q^2,\mu_R^2,\mu_F^2)$ gives a good approximation to the complete sum $F_\pi(Q^2)$.

It should be noted that in $F_\pi^{(0)}(Q^2,\mu_R^2,\mu_F^2)$, given by Eq. (4.2), μ_R appears only through $\alpha_S(\mu_R^2)$, whereas μ_F enters into the distribution amplitude $\phi(x,\mu_F^2)$. In $F_\pi^{(1)}(Q^2,\mu_R^2,\mu_F^2)$, given by Eqs. (4.3)–(4.5), a logarithmic dependence on the scales μ_R and μ_F appears also through $T_H^{(1)}(x,y,\mu_R^2/Q^2,\mu_F^2/Q^2)$. As seen from Eqs. (2.21) and (2.20), this dependence is contained in the terms

$$f_{UV}(x,y,Q^2/\mu_R^2)=\frac{1}{4}\beta_0\left[\frac{5}{3}-\ln(\overline{xy})+\ln\frac{\mu_R^2}{Q^2}\right], \tag{4.7}$$

$$f_{IR}(x,y,Q^2/\mu_F^2)=\frac{2}{3}[3+\ln(\overline{xy})]\left[\frac{1}{2}\ln(\overline{xy})-\ln\frac{\mu_F^2}{Q^2}\right]. \tag{4.8}$$

Being independent of each other, the scales μ_R and μ_F can be expressed in terms of Q^2 as

$$\mu_R^2=a(x,y)Q^2, \tag{4.9}$$

$$\mu_F^2=b(x,y)Q^2, \tag{4.10}$$

where $a(x,y)$ and $b(x,y)$ are some linear functions of the dimensionless variables x and y (quark longitudinal momentum fractions).

We next discuss various possibilities of choosing the scales μ_R and μ_F separately. The simplest and widely used choice for the scale μ_R is

$$\mu_R^2=Q^2, \tag{4.11}$$

the justification for the use of which is mainly pragmatic.

Physically, however, the more appropriate choice for μ_R^2 would be that one corresponding to the characteristic virtualities of the particles in the parton subprocess, which is considerably lower than the overall momentum transfer Q^2 (i.e., virtuality of the probing photon).

It follows from Figs. 1 and 2 that the virtualities of the gluon line (line 4) and the internal quark line (line 2) of diagram A in Fig. 2 are given by $\overline{xy}Q^2$ and $\overline{y}Q^2$, respectively. Now, if instead of using Eq. (4.11) we choose μ_R to be equal to the gluon virtuality, i.e.,

$$\mu_R^2=\overline{xy}Q^2, \tag{4.12}$$

then the logarithmic terms in Eq. (4.7) vanish.

As it is well known, unlike in an Abelian theory (e.g., QED), where the effective coupling is entirely renormalized by the corrections of the vector particle propagator, in QCD the coupling is renormalized not only by the gluon propagator, but also by the quark-gluon vertex and quark-propagator corrections. It is thus possible to choose μ_R^2 as the geometrical mean of the gluon and quark virtualities [6]:

$$\mu_R^2=\sqrt{(\overline{xy}Q^2)(\overline{y}Q^2)}. \tag{4.13}$$

Alternatively, we can make a choice

$$\mu_R^2=e^{-5/3}\overline{xy}Q^2, \tag{4.14}$$

as a result of which the function f_{UV}, given by Eq. (4.7), vanishes identically. In this case, $T_H^{(1)}(x,y,\mu_R^2/Q^2,\mu_F^2/Q^2)$ defined by Eq. (2.20) becomes n_f independent. This is an example of choosing the renormalization scale according to the Brodsky-Lepage-Mackenzie (BLM) procedure [28]. In this procedure, the renormalization scale μ_R^2 best suited to a particular process in a given order can be determined by computing vacuum-polarization insertions in the diagrams of that order. The essence of the BLM procedure is that all vacuum-polarization effects from the QCD β function are resummed into the running coupling constant.

Let us just mention at this point that in addition to the BLM procedure, two more renormalization scale-setting procedures in PQCD have been proposed in the literature: the principle of fastest apparent convergence (FAC) [29], and the principle of minimal sensitivity (PMS) [30]. The application of those three quite distinct methods can give strikingly different results in practical calculations [31].

As for the factorization scale μ_F^2, it basically determines how much of the collinear term given in Eq. (4.8), is absorbed into the distribution amplitude. A natural choice for this scale would be

$$\mu_F^2=Q^2, \tag{4.15}$$

which eliminates the logarithms of Q^2/μ_F^2. More preferable to Eq. (4.15) is the choice

$$\mu_F^2=\sqrt{\overline{xy}}Q^2, \tag{4.16}$$

which makes the function f_{IR}, given by Eq. (4.8), vanish.

A glance at Eqs. (4.1)–(4.5), where the coupling constants $\alpha_S(\mu_R^2)$ and $\alpha_S(\mu_F^2)$ appear under the integral sign, reveals that any of the choices of μ_R given by Eqs. (4.12)–(4.14), and the choice of μ_F given by Eq. (4.16), leads immediately to the problem if the usual one-loop formula (2.2) for the effective QCD running coupling constant is employed. Namely, then, regardless of how large Q^2 is, the integration of Eqs. (4.1)–(4.5) allows $\alpha_S(\mu_R^2)$ to be evaluated near zero momentum transfer. Two approaches are possible to circumvent this problem. First, one can choose μ_R^2 and μ_F^2 to be effective constants by taking $\mu_R^2=\langle\mu_R^2\rangle$ and $\mu_F^2=\langle\mu_F^2\rangle$, respectively. Second, one can introduce a cutoff in formula (2.2) with the aim of preventing the effective coupling from becoming infinite for vanishing gluon momenta.

If the first approach is taken, Eqs. (4.12)–(4.14) and (4.16) get replaced by the averages

$$\mu_R^2=\langle\overline{xy}Q^2\rangle, \tag{4.17a}$$

$$\mu_R^2=\sqrt{\langle\overline{xy}Q^2\rangle\langle\overline{y}Q^2\rangle}, \tag{4.17b}$$

$$\mu_R^2=\langle e^{-5/3}\overline{xy}Q^2\rangle, \tag{4.17c}$$

and

$$\mu_F^2=\sqrt{\langle\overline{xy}\rangle}Q^2, \tag{4.18}$$

respectively. Taking into account the fact that $\langle\overline{xy}\rangle=\langle\overline{x}\rangle\langle\overline{y}\rangle$ and $\langle\overline{x}\rangle=\langle\overline{y}\rangle$, it is possible to write Eqs. (4.17) and (4.18) in the respective forms

$$\mu_R^2=\langle\overline{x}\rangle^2Q^2, \tag{4.19a}$$

$$\mu_R^2=\langle\overline{x}\rangle^{3/2}Q^2, \tag{4.19b}$$

$$\mu_R^2 = e^{-5/3}\langle\overline{x}\rangle^2 Q^2, \tag{4.19c}$$

and

$$\mu_F^2 = \langle\overline{x}\rangle Q^2. \tag{4.20}$$

The key quantity in the above considerations is $\langle\overline{x}\rangle$, the average value of the momentum fraction. It depends on the form of the distribution amplitude, and there is no unique way of defining it. A possible definition is

$$\langle\overline{x}\rangle(\mu_F^2) = \frac{\int_0^1 dx\, \phi(x,\mu_F^2)\overline{x}}{\int_0^1 dx\, \phi(x,\mu_F^2)}. \tag{4.21}$$

Owing to the fact that all distribution amplitudes under consideration are centered around the value $x=0.5$, it follows trivially from Eq. (4.21) that for all of them

$$\langle\overline{x}\rangle(\mu_F^2) = 0.5. \tag{4.22}$$

An alternative way of defining $\langle\overline{x}\rangle$, motivated by the form of the LO expression for the pion form factor (4.6), is

$$\langle\overline{x}\rangle(\mu_F^2) = \frac{\int_0^1 dx\, \dfrac{\phi^{LO}(x,\mu_F^2)}{\overline{x}}\,\overline{x}}{\int_0^1 dx\, \dfrac{\phi^{LO}(x,\mu_F^2)}{\overline{x}}} = \frac{1}{3[1+B_2^{LO}(\mu_F^2)+B_4^{LO}(\mu_F^2)+\ldots]}. \tag{4.23}$$

It should be noted, however, that this formula can be straightforwardly applied only if $\mu_F^2 = Q^2$. On the other hand, if instead of $\mu_F^2 = Q^2$ one chooses the factorization scale to be as given by Eq. (4.20), then Eqs. (4.20) and (4.23) form a nontrivial system of simultaneous equations. According to Eq. (4.23), one obtains $\langle\overline{x}\rangle_{as}(Q^2) = 1/3$ for any Q^2, while $0.242 \leqslant \langle\overline{x}\rangle_{CZ}(Q^2) \leqslant 0.262$ for $4\ \mathrm{GeV}^2 \leqslant Q^2 \leqslant 100\ \mathrm{GeV}^2$ (similar values are obtained for ϕ_{P2} and ϕ_{P3}).

When using the $\phi_{as}(x,\mu_F^2)$ distribution it appears reasonable to take $\langle\overline{x}\rangle(\mu_F^2) = \langle\overline{x}\rangle_{as} = 1/2$. This can be justified on the grounds that this distribution is concentrated around $x=0.5$, and is characterized by a very weak evolution. On the other hand, for the end-point concentrated distributions $\phi_{CZ}(x,\mu_F^2)$, $\phi_{P2}(x,\mu_F^2)$ and $\phi_{P3}(x,\mu_F^2)$, which exhibit sizable evolutional effects, it is more appropriate to take $\langle\overline{x}\rangle(\mu_F^2)$ as given by Eq. (4.23).

As stated above, the divergence of the effective QCD coupling $\alpha_S(\mu_R^2)$, as given by Eq. (2.2), is the reason that it is not possible to use the choices of μ_R^2 given by Eqs. (4.12)–(4.14) and μ_F^2 given by Eq. (4.16). Equation (2.2) does not represent the nonperturbative behavior of $\alpha_S(\mu_R^2)$ for small μ_R^2, and a number of proposals have been suggested for the form of the coupling constant in this regime [32]. The most exploited parametrization of the effective QCD coupling constant at low energies has the form

$$\alpha_S(\mu_R^2) = \frac{4\pi}{\beta_0 \ln\left(\dfrac{\mu_R^2 + C^2}{\Lambda^2}\right)}, \tag{4.24}$$

where the constant C encodes the nonperturbative dynamics and is usually interpreted as an ''effective dynamical gluon mass'' m_g. For $\mu_R^2 \gg C^2$, the effective coupling in Eq. (4.24) coincides with the one-loop formula (2.2), whereas at low momentum transfer this formula ''freezes'' to some finite but not necessarily small value.

In view of the confinement phenomenon, the modification (4.24) is very natural: the lower bound on the particle momenta is set by the inverse of the confinement radius. This is equivalent to a strong suppression for the propagation of particles with small momenta. Thus, in a consistent calculation in which Eq. (4.24) is assumed a modified gluon propagator should be used:

$$\frac{1}{k^2} \to \frac{1}{k^2 - m_g^2}. \tag{4.25}$$

However, if one attempts to calculate the LO prediction for the pion form factor making use of Eqs. (4.24) and (4.25), and taking $m_g = 300-500$ MeV, the result obtained is by a factor of 10 lower than the experimental value, questioning the applicability of such an approach [15].

It has recently been shown that spontaneous chiral symmetry breaking imposes rather a severe restriction on the idea of freezing [33]. The authors of [33] argue that before any argument based on a particular form of the freezing coupling constant is put forward, one should check that the dynamical origin (mechanism) of the freezing is such that enough chiral symmetry breaking can be produced.

Considering the discussion above, calculations with the frozen coupling constant seem to need a more refined treatment and will not be considered in this paper.

V. COMPLETE NLO NUMERICAL PREDICTIONS FOR THE PION FORM FACTOR

Having obtained all the necessary ingredients in the preceding sections, now we put them together and obtain complete leading-twist NLO QCD numerical predictions for the pion form factor. For a fixed distribution amplitude, we analyze the dependence of our results on the choice of the scales μ_R and μ_F.

By inserting Eqs. (3.18) and (3.20) into Eqs. (4.2) and (4.5), taking into account Eq. (2.4), taking the scales μ_R^2 and μ_F^2 to be effective constants (as explained in Sec. IV), and performing the x and y integration, we find that Eqs. (4.2) and (4.5) take the form

$$Q^2F_\pi^{(0)}(Q^2,\mu_R^2,\mu_F^2)=8\pi f_\pi^2\alpha_S(\mu_R^2)\left(\sum_{n=0}^{\infty}{}'B_n^{LO}(\mu_F^2)\right)^2, \tag{5.1}$$

and

$$Q^2F_\pi^{(1b)}(Q^2,\mu_R^2,\mu_F^2)=16f_\pi^2\alpha_S(\mu_R^2)\alpha_S(\mu_F^2)\left(\sum_{n=0}^{\infty}{}'B_n^{LO}(\mu_F^2)\right)\left(\sum_{k=2}^{\infty}{}'B_k^{NLO}(\mu_F^2)\right). \tag{5.2}$$

For a distribution amplitude of the form given in Eqs. (3.25)–(3.30), the above expression reduces to

$$Q^2F_\pi^{(0)}(Q^2,\mu_R^2,\mu_F^2)=8\pi f_\pi^2\alpha_S(\mu_R^2)[1+B_2^{LO}(\mu_F^2)+B_4^{LO}(\mu_F^2)]^2, \tag{5.3}$$

$$Q^2F_\pi^{(1b)}(Q^2,\mu_R^2,\mu_F^2)=16f_\pi^2\alpha_S(\mu_R^2)\alpha_S(\mu_F^2)[1+B_2^{LO}(\mu_F^2)+B_4^{LO}(\mu_F^2)] \times\left[B_2^{NLO}(\mu_F^2)+B_4^{NLO}(\mu_F^2)+\sum_{k=6}^{\infty}{}'B_k^{NLO}(\mu_F^2)\right]. \tag{5.4}$$

As for the part of the NLO contribution arising from the NLO correction to the hard-scattering amplitude, by inserting Eqs. (2.20) and (3.27) into Eq. (4.4) and performing the x and y integration one obtains

$$\begin{aligned}Q^2F_\pi^{(1a)}(Q^2,\mu_R^2,\mu_F^2)=8f_\pi^2\alpha_S^2(\mu_R^2)\Bigg\{&\frac{9}{4}[1+B_2^{LO}(\mu_F^2)+B_4^{LO}(\mu_F^2)]^2\ln\frac{\mu_R^2}{Q^2}+\frac{2}{3}\left[\frac{25}{6}B_2^{LO}(\mu_F^2)+\frac{91}{15}B_4^{LO}(\mu_F^2)\right]\\ &\times[1+B_2^{LO}(\mu_F^2)+B_4^{LO}(\mu_F^2)]\ln\frac{\mu_F^2}{Q^2}+6.58+24.99B_2^{LO}(\mu_F^2)+21.43(B_2^{LO}(\mu_F^2))^2\\ &+32.81B_4^{LO}(\mu_F^2)+32.55(B_4^{LO}(\mu_F^2))^2+53.37B_2^{LO}(\mu_F^2)B_4^{LO}(\mu_F^2)\Bigg\}.\end{aligned} \tag{5.5}$$

Then the NLO contribution to the ''almost scaling'' combination $Q^2F_\pi(Q^2)$ is given by

$$Q^2F_\pi^{(1)}(Q^2,\mu_R^2,\mu_F^2)=Q^2F_\pi^{(1a)}(Q^2,\mu_R^2,\mu_F^2)+Q^2F_\pi^{(1b)}(Q^2,\mu_R^2,\mu_F^2), \tag{5.6}$$

while the total NLO prediction reads

$$Q^2F_\pi(Q^2,\mu_R^2,\mu_F^2)=Q^2F_\pi^{(0)}(Q^2,\mu_R^2,\mu_F^2)+Q^2F_\pi^{(1)}(Q^2,\mu_R^2,\mu_F^2). \tag{5.7}$$

For the purpose of this calculation we adopt the criteria according to which a perturbative prediction for $F_\pi(Q^2)$ is considered reliable provided the following two requirements are met: first, corrections to the LO prediction are reasonably small ($<30\%$); second, the expansion parameter (effective QCD coupling constant) is acceptably small [$\alpha_S(\mu_R^2)<0.3$ or 0.5]. Of course, one more requirement should be added to the above ones: consistency with experimental data. This requirement, however, is not of much use here since reliable experimental data for the pion form factor exist for $Q^2\leqslant 4$ GeV^2, i.e., well outside the region in which the perturbative treatment based on Eq. (1.1) is justified.

Currently available experimental data for the spacelike pion electromagnetic form factor $F_\pi(Q^2)$ are shown in Fig. 7. The data are taken from Bebek *et al.* [34] and Amendolia *et al.* [35]. As stated in [34], the measurements corresponding to $Q^2=6.30$ GeV^2 and $Q^2=9.77$ GeV^2 are somewhat questionable. Thus, effectively, the data for $F_\pi(Q^2)$ exist only for Q^2 in the range $Q^2\leqslant 4$ GeV^2. The results of Ref. [34] were obtained from the extrapolation of the $\gamma^*p\rightarrow\pi^+n$ electroproduction data to the pion pole. It should also be mentioned that the analysis of Ref. [34] is subject to criticism which questions whether $F_\pi(Q^2)$ was truly determined for $1\leqslant Q^2\leqslant 4$ GeV^2 [36] (but see also Ref. [37]). The new data in this energy region are expected from the CEBAF experiment E-93-021.

A. Predictions obtained with $\mu_R^2=\mu_F^2=Q^2$

The first NLO prediction for the pion form factor was obtained in Ref. [5]. Using the $\overline{\rm MS}$ renormalization scheme and the choice $\mu_R^2=\mu_F^2=Q^2$ it was found that for the $\phi_{as}(x)$ distribution (with the evolution of the distribution amplitude neglected), the perturbative series took the form

$$Q^2F_\pi(Q^2)=(0.43\text{GeV}^2)\alpha_S(Q^2)[1+2.10\alpha_S(Q^2)+\cdots], \tag{5.8}$$

which is in agreement with our result given by Eqs. (5.7),

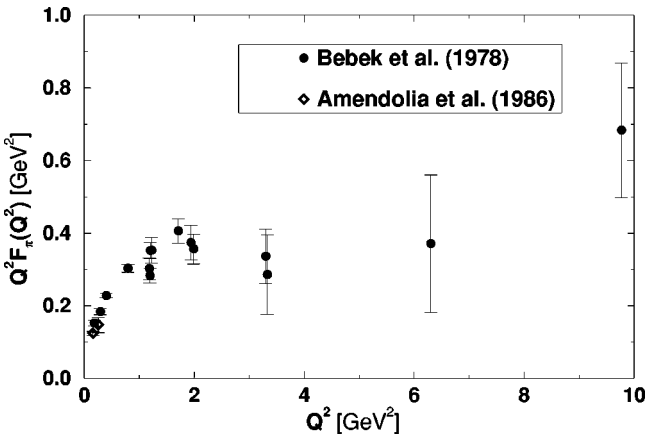

FIG. 7. Presently available experimental data for the spacelike pion electromagnetic form factor.

(5.3), and (5.5). The conclusion based on this result was that a reliable result for $F_\pi(Q^2)$ was not obtained until $\alpha_S(Q^2) \approx 0.1$, or with $\Lambda_{\overline{\rm MS}}=0.5$ GeV, $Q^2=10000$ GeV^2. This prediction has been widely cited in the literature and initiated a lot of discussion regarding the applicability of PQCD to the calculation of exclusive processes at large momentum transfer. With the presently accepted value of 0.2 GeV for $\Lambda_{\overline{\rm MS}}$, we find that the criteria from Ref. [5] are satisfied for $Q^2 \sim 1600$ GeV^2, and that for $Q^2=700$ GeV^2, the corrections to the LO prediction are of order 30%. Thus, this result shows that for the choice of the renormalization and factorization scales $\mu_R^2=\mu_F^2=Q^2$, the region in which perturbative predictions can be considered reliable is still well beyond the region in which experimental data exist. The inclusion of the distribution amplitude evolution effects, although extremely important for the end-point concentrated amplitudes, does not change this conclusion.

Numerical results of our complete NLO QCD calculation, obtained using the four candidate distribution amplitudes, with $\mu_R^2=\mu_F^2=Q^2$, and for $Q^2 \geqslant 4$ GeV^2, are displayed in Tables II, III, IV, and V. The entries in these tables include various contributions given by Eqs. (5.3)–(5.7), comprising the full NLO result. A comparison of our results with presently available experimental data is shown in Fig. 8. The ratio of the NLO to the LO contribution to $F_\pi(Q^2)$, i.e., $F_\pi^{(1)}(Q^2)/F_\pi^{(0)}(Q^2)$, as a useful measure of the importance of the NLO corrections, is plotted as a function of Q^2 in Fig. 9. The shaded areas appearing in Figs. 8 and 9 denote the region of Q^2 where $\alpha_S(Q^2)>0.3$. We take that outside of this region the effective coupling is acceptably small.

It is evident from Figs. 8 and 9 and Tables II–V that the leading-twist NLO results for the pion form factor obtained with $\mu_R^2=\mu_F^2=Q^2$ display the following general features. First, the results are quite sensitive to the assumed form of the pion distribution amplitude. Thus, the more end-point concentrated distribution amplitude is, the larger result for the pion form factor is obtained, and also the NLO corrections are larger [which has already been obvious looking at Eqs. (5.3)–(5.7)]. Second, whereas the NLO correction arising from the corrections to the hard-scattering amplitude are positive, the corrections due to the inclusion of the evolutional corrections to the distribution amplitude are negative, with the former being generally an order of magnitude larger than the latter. Thus, in all the cases considered, the full NLO correction to the pion form factor is positive, i.e., its inclusion increases the LO prediction.

We now briefly comment on the results obtained with each of the four distribution amplitudes.

Table II, which corresponds to the $\phi_{as}(x,Q^2)$ distribution amplitude, shows that the NLO correction $Q^2F_\pi^{(1)}(Q^2)$ is rather large (36% at $Q^2=100$ GeV^2). Most of the contribution to $Q^2F_\pi^{(1)}(Q^2)$ is due to the NLO correction to the hard-scattering amplitude $Q^2F_\pi^{(1a)}(Q^2)$, while the contribution $Q^2F_\pi^{(1b)}(Q^2)$ arising from the NLO evolutional correction of the distribution amplitude is rather small, being of order 1%. The ratio $F_\pi^{(1)}(Q^2)/F_\pi^{(0)}(Q^2) \approx 30\%$ is reached at $Q^2 \approx 500$ GeV^2.

The results derived from the $\phi_{CZ}(x,Q^2)$ distribution are presented in Table III. The full NLO correction $Q^2F_\pi^{(1)}(Q^2)$ is somewhat larger than for $\phi_{as}(x,Q^2)$ (and at $Q^2=100$ GeV^2 it amounts to 46%). The ratio $F_\pi^{(1)}(Q^2)/F_\pi^{(0)}(Q^2)$ is greater than 30% until $Q^2 \approx 2400$ GeV^2. It is important to observe that the evolutional

TABLE II. Complete leading-twist NLO QCD results for the pion form factor, $Q^2F_\pi(Q^2)$, obtained using the $\phi_{as}(x,\mu_F^2)$ distribution amplitude and assuming $\mu_R^2=\mu_F^2=Q^2$.

Q^2 [GeV^2]	$\alpha_S(\mu_R^2)$	$Q^2F_\pi^{(0)}(Q^2)$ [GeV^2]	$Q^2F_\pi^{(1a)}(Q^2)$ [GeV^2]	$Q^2F_\pi^{(1b)}(Q^2)$ [GeV^2]	$Q^2F_\pi^{(1)}(Q^2)$ [GeV^2]	$F_\pi^{(1)}(Q^2)/F_\pi^{(0)}(Q^2)$ %	$Q^2F_\pi(Q^2)$ [GeV^2]
4	0.303	0.131	0.083	-0.001	0.082	62.8	0.213
6	0.279	0.120	0.070	-0.001	0.069	57.6	0.189
8	0.264	0.114	0.063	-0.001	0.062	54.4	0.176
10	0.253	0.109	0.058	-0.001	0.057	52.2	0.166
20	0.225	0.097	0.046	-0.001	0.045	46.2	0.142
30	0.211	0.091	0.040	-0.001	0.039	43.3	0.130
40	0.202	0.087	0.037	-0.001	0.036	41.4	0.123
50	0.196	0.085	0.035	-0.001	0.034	40.1	0.118
75	0.185	0.080	0.031	-0.001	0.030	37.9	0.110
100	0.178	0.077	0.029	-0.001	0.028	36.4	0.105

TABLE III. Same as Table II but for the $\phi_{CZ}(x,\mu_F^2)$ distribution amplitude.

Q^2 [GeV^2]	$\alpha_S(\mu_R^2)$	$Q^2F_\pi^{(0)}(Q^2)$ [GeV^2]	$Q^2F_\pi^{(1a)}(Q^2)$ [GeV^2]	$Q^2F_\pi^{(1b)}(Q^2)$ [GeV^2]	$Q^2F_\pi^{(1)}(Q^2)$ [GeV^2]	$F_\pi^{(1)}(Q^2)/F_\pi^{(0)}(Q^2)$ %	$Q^2F_\pi(Q^2)$ [GeV^2]
4	0.303	0.248	0.241	-0.015	0.225	90.8	0.474
6	0.279	0.222	0.195	-0.014	0.181	81.6	0.403
8	0.264	0.206	0.170	-0.013	0.157	76.1	0.363
10	0.253	0.195	0.153	-0.012	0.141	72.2	0.336
20	0.225	0.167	0.115	-0.011	0.104	62.2	0.271
30	0.211	0.154	0.098	-0.010	0.088	57.4	0.243
40	0.202	0.146	0.089	-0.009	0.079	54.3	0.225
50	0.196	0.140	0.082	-0.009	0.073	52.2	0.213
75	0.185	0.131	0.072	-0.008	0.064	48.7	0.194
100	0.178	0.125	0.065	-0.008	0.058	46.4	0.182

corrections, especially the LO ones, are rather significant in this case. Also, as it is seen from Table III, the NLO evolutional correction $Q^2F_\pi^{(1b)}(Q^2)$ is of order $\approx 6\%$, i.e., nonnegligible. To show the importance of the correction arising from the inclusion of the distribution amplitude evolution, the results for $Q^2F_\pi(Q^2)$ and the ratio $F_\pi^{(1)}(Q^2)/F_\pi^{(0)}(Q^2)$ obtained using the $\phi_{CZ}(x)$, $\phi_{CZ}^{LO}(x,Q^2)$, and $\phi_{CZ}(x,Q^2)$ distributions, are exhibited in Figs. 10 and 11, respectively.

The results based on the $\phi_{P2}(x,Q^2)$ and $\phi_{P3}(x,\mu_F^2)$ distributions are listed in Tables IV and V, respectively. As it can be easily seen by looking at Figs. 8 and 9 and by comparing the corresponding entries in Tables III and IV, the results obtained with the $\phi_{P2}(x,Q^2)$ and $\phi_{CZ}(x,Q^2)$ distributions are practically the same qualitatively, while differ quantitatively by a few percent. From Table V and Figs. 8 and 9, one can see that the behavior of the results obtained with the $\phi_{P3}(x,\mu_F^2)$ distribution is qualitatively similar to the behavior of the results obtained with other two end-point concentrated distributions. For this reason, we leave the $\phi_{P2}(x,Q^2)$ and $\phi_{P3}(x,\mu_F^2)$ distributions out of our further consideration.

In view of what has been said above, we may conclude the following. If the pion is modeled by the $\phi_{as}(x,\mu_F^2)$, $\phi_{CZ}(x,\mu_F^2)$, $\phi_{P2}(x,\mu_F^2)$, or $\phi_{P3}(x,\mu_F^2)$ distribution amplitude, and if the renormalization and factorization scale are chosen to be $\mu_R^2=\mu_F^2=Q^2$, one finds that the NLO corrections to the lowest-order prediction for the pion form factor are large. The NLO predictions obtained cannot be made reliable, i.e., $F_\pi^{(1)}(Q^2)/F_\pi^{(0)}(Q^2)$ less than, say, 30%, until the momentum transfer $Q \gg 10$ GeV is reached. Based on these findings and considering the region of Q^2 in which the data exist, it is clear that we are not in a position to rule out any of the four distributions considered. One can only note that the predictions for $Q^2F_\pi(Q^2,\mu_R^2,\mu_F^2)$ obtained with the $\phi_{as}(x,\mu_F^2)$ distribution are below the trend indicated by the existing experimental data, while the end-point concentrated distributions $\phi_{CZ}(x,\mu_F^2)$, $\phi_{P2}(x,\mu_F^2)$, and $\phi_{P3}(x,\mu_F^2)$ give higher predictions. It is worth mentioning here that the theoretical predictions for the photon-to-pion transition form factor $F_{\pi\gamma}(Q^2)$ are in very good agreement with the data, assuming the pion distribution amplitude is close to the asymptotic one, i.e., $\phi_{as}(x,\mu_F^2)$ [38].

B. Predictions obtained using $\mu_R^2=aQ^2$ and $\mu_F^2=bQ^2$

In this subsection we present a detailed analysis of the dependence of the complete leading-twist NLO predictions for the pion form factor on the renormalization and factorization scales, μ_R and μ_F. Being a reflection of the uncalculated higher-order contributions, this dependence is a very

TABLE IV. Same as Table II but for the $\phi_{P2}(x,\mu_F^2)$ distribution amplitude.

Q^2 [GeV^2]	$\alpha_S(\mu_R^2)$	$Q^2F_\pi^{(0)}(Q^2)$ [GeV^2]	$Q^2F_\pi^{(1a)}(Q^2)$ [GeV^2]	$Q^2F_\pi^{(1b)}(Q^2)$ [GeV^2]	$Q^2F_\pi^{(1)}(Q^2)$ [GeV^2]	$F_\pi^{(1)}(Q^2)/F_\pi^{(0)}(Q^2)$ %	$Q^2F_\pi(Q^2)$ [GeV^2]
4	0.303	0.274	0.278	-0.019	0.259	94.6	0.532
6	0.279	0.244	0.224	-0.017	0.207	85.0	0.451
8	0.264	0.226	0.195	-0.016	0.179	79.1	0.404
10	0.253	0.213	0.175	-0.015	0.160	75.0	0.374
20	0.225	0.182	0.130	-0.013	0.117	64.5	0.300
30	0.211	0.167	0.111	-0.012	0.100	59.4	0.267
40	0.202	0.158	0.100	-0.011	0.089	56.2	0.247
50	0.196	0.152	0.093	-0.011	0.082	54.0	0.234
75	0.185	0.141	0.081	-0.010	0.071	50.2	0.212
100	0.178	0.134	0.074	-0.009	0.064	47.9	0.199

TABLE V. Same as Table II but for the $\phi_{P3}(x,\mu_F^2)$ distribution amplitude.

Q^2 [GeV^2]	$\alpha_S(\mu_R^2)$	$Q^2F_\pi^{(0)}(Q^2)$ [GeV^2]	$Q^2F_\pi^{(1a)}(Q^2)$ [GeV^2]	$Q^2F_\pi^{(1b)}(Q^2)$ [GeV^2]	$Q^2F_\pi^{(1)}(Q^2)$ [GeV^2]	$F_\pi^{(1)}(Q^2)/F_\pi^{(0)}(Q^2)$ %	$Q^2F_\pi(Q^2)$ [GeV^2]
4	0.303	0.335	0.402	-0.029	0.372	111.0	0.708
6	0.279	0.295	0.318	-0.026	0.292	100.0	0.587
8	0.264	0.272	0.273	-0.024	0.249	91.8	0.521
10	0.253	0.255	0.244	-0.023	0.222	86.7	0.477
20	0.225	0.215	0.178	-0.019	0.158	73.8	0.373
30	0.211	0.196	0.150	-0.017	0.133	67.7	0.328
40	0.202	0.184	0.134	-0.016	0.118	63.8	0.302
50	0.196	0.176	0.123	-0.015	0.108	61.1	0.284
75	0.185	0.163	0.106	-0.014	0.092	56.6	0.255
100	0.178	0.154	0.096	-0.013	0.083	53.7	0.237

important feature of the NLO predictions, and can therefore be used as a guide to assess their accuracy.

In the following we shall restrict our attention to the two most exploited pion distribution amplitudes $\phi_{as}(x,\mu_F^2)$ and $\phi_{CZ}(x,\mu_F^2)$.

In the preceding subsection, we have found that the NLO corrections calculated using these two distributions are large, especially for the latter. The reason for this lies in the fact that the renormalization scale choice $\mu_R^2=Q^2$ is not an appropriate one. Namely, owing to the partitioning of the overall momentum transfer Q^2 among the particles in the parton subprocess, the essential virtualities of the particles are smaller than Q^2, so that the physical renormalization scale, better suited for analyzing the process under consideration, is inevitably lower than the external scale Q^2.

A characteristic feature of the asymptotic distribution $\phi_{as}(x,\mu_F^2)$ is that in the LO it shows no evolution. A consequence of this, as it can be seen from Eqs. (5.3)–(5.7), is that the NLO predictions for the pion form factor based on this distribution are essentially independent of the factorization scale μ_F. Namely, the only dependence on this scale is contained in the term arising from the NLO evolutional effects, which are tiny, as we have seen in Sec. III. On the other hand, the predictions calculated with the $\phi_{CZ}(x,\mu_F^2)$ are μ_F dependent, but this dependence turns out to be very weak. Thus, for a given value of μ_R, variation of the value of μ_F in the range $Q^2/4\leqslant\mu_F^2\leqslant Q^2$ leads to practically the same results.

Therefore, by examining the NLO predictions based on the $\phi_{as}(x,\mu_F^2)$ and $\phi_{CZ}(x,\mu_F^2)$ distributions, we find that they depend very little on the factorization scale μ_F. Consequently, when using these distributions one is allowed to set $\mu_F^2=Q^2$, for all practical purposes.

1. Examining the renormalization scale dependence of the NLO corrections

The three specific physically motivated choices of μ_R, given by Eq. (4.19), can be conveniently written as

$$\mu_R^2=aQ^2, \tag{5.9a}$$

where

$$a\in\{\langle\overline{x}\rangle^{3/2},\langle\overline{x}\rangle^2,e^{-5/3}\langle\overline{x}\rangle^2\}. \tag{5.9b}$$

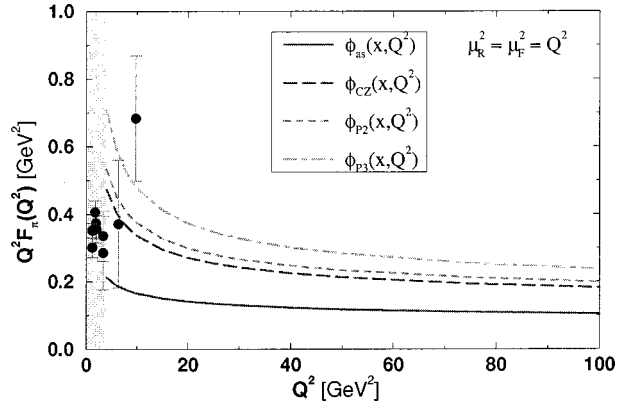

FIG. 8. Comparison of the complete leading-twist NLO QCD predictions for the pion form factor, $Q^2F_\pi(Q^2)$, obtained using the four candidate distribution amplitudes, with the presently available experimental data. The shaded area denotes the region of Q^2 in which $\alpha_S(Q^2)>0.3$.

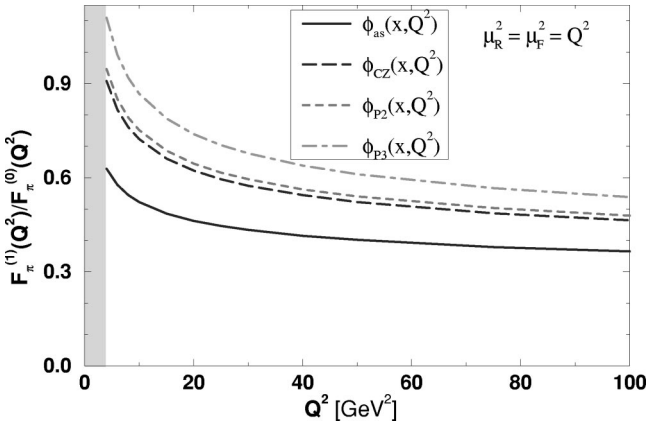

FIG. 9. The ratio of the NLO to the LO contributions to the pion form factor, $F_\pi^{(1)}(Q^2)/F_\pi^{(0)}(Q^2)$, for the four candidate distribution amplitudes. The shaded area denotes the region of Q^2 in which $\alpha_S(Q^2)>0.3$.

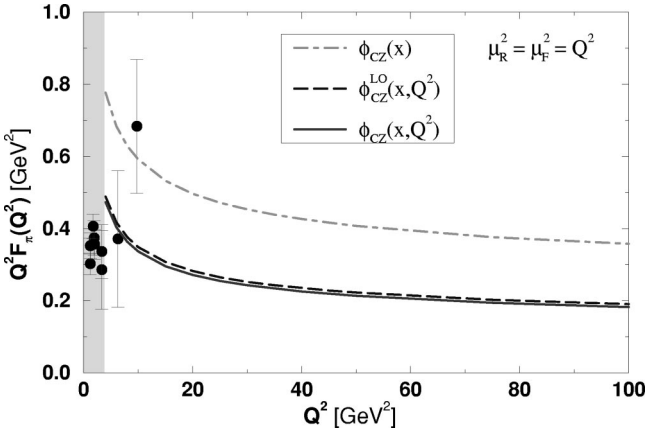

FIG. 10. Leading-twist NLO QCD predictions for the pion form factor, $Q^2F_\pi(Q^2)$, obtained with the $\phi_{CZ}(x)$, $\phi_{CZ}^{LO}(x,Q^2)$, and $\phi_{CZ}(x,Q^2)$ distributions. The shaded area denotes the region of Q^2 in which $\alpha_S(Q^2)>0.3$.

For the purpose of the discussion of the effects of the inclusion of the NLO corrections on the LO predictions, we have included Fig. 12 showing the LO predictions for the three different values of μ_R given in Eq. (5.9). Our complete leading-twist NLO predictions for the pion form factor calculated with the $\phi_{as}(x,\mu_F^2)$ distribution and with the three specific values of the renormalization scale μ_R are summarized in Figs. 13 and 14, showing the results for $Q^2F_\pi(Q^2)$ and the ratio $F_\pi^{(1)}(Q^2)/F_\pi^{(0)}(Q^2)$, respectively. The corresponding results obtained assuming the $\phi_{CZ}(x,\mu_F^2)$ distribution are displayed in Figs. 15, 16, and 17.

The solid curves in Figs. 12–17 correspond to the results, with $\mu_R^2=\mu_F^2=Q^2$ obtained in the preceding subsection, are included for comparison. The other curves refer to the choices of μ_R^2 given by Eq. (5.9).

Some general comments concerning the results presented above are in order. First of all, it is interesting to note that the predictions based on the $\phi_{as}(x,\mu_F^2)$ and $\phi_{CZ}(x,\mu_F^2)$ distributions amplitudes almost share the qualitative features, al-

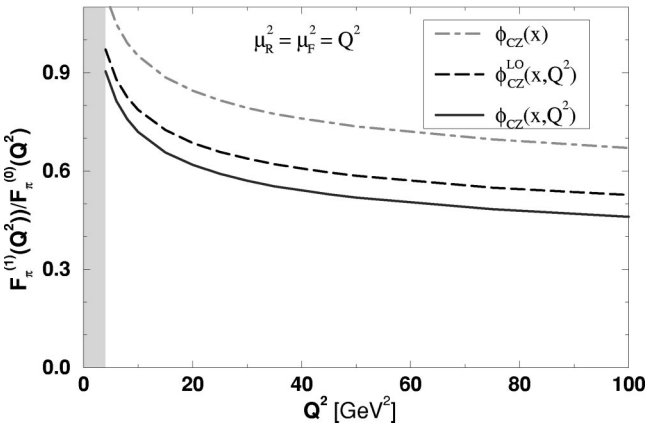

FIG. 11. The ratio of the NLO to the LO contributions to the pion form factor, $F_\pi^{(1)}(Q^2)/F_\pi^{(0)}(Q^2)$, obtained for the $\phi_{CZ}(x)$, $\phi_{CZ}^{LO}(x,Q^2)$, and $\phi_{CZ}(x,Q^2)$ distributions. The shaded area denotes the region of Q^2 in which $\alpha_S(Q^2)>0.3$.

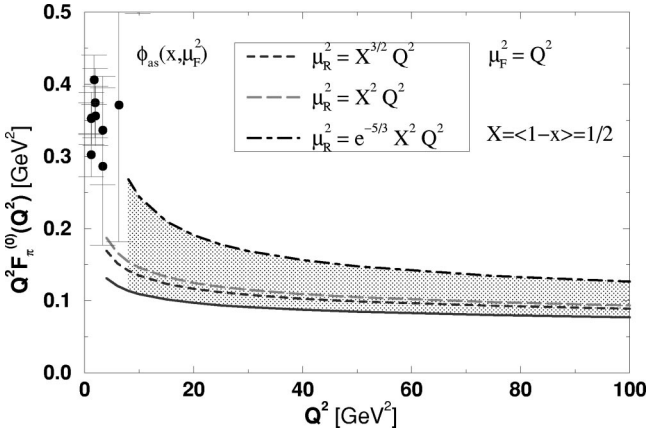

FIG. 12. The numerical results for $Q^2F_\pi^{(0)}(Q^2)$ obtained with the $\phi_{as}(x,\mu_F^2)$ distribution amplitude and the choices of μ_R^2 given by Eq. (4.19), with $\mu_F^2=Q^2$ and $\langle\overline{x}\rangle_{as}=1/2$. The solid curve (included for comparison) corresponds to the case $\mu_R^2=\mu_F^2=Q^2$ considered in the preceding subsection. The shaded area denotes the range of the LO prediction $Q^2F_\pi^{(0)}(Q^2)$ for $\mu_R^2/Q^2\in[e^{-5/3}\langle\overline{x}\rangle^2,1]$.

though these two distributions are quite different in shape. Next, by looking at Figs. 13 and 16, one notices that the full NLO result for $Q^2F_\pi(Q^2)$ shows a very weak dependence on the value of μ_R^2, and that it increases with decreasing μ_R^2. As far as the ratio $F_\pi^{(1)}(Q^2)/F_\pi^{(0)}(Q^2)$ is concerned, as evident from Figs. 14 and 17, the situation is quite different. It is rather sensitive to the variation of μ_R^2, and decreases as μ_R^2 decreases. The choice $\mu_R^2=Q^2$, represented by solid curves, when compared with the other possibilities considered, leads to the lowest value for $Q^2F_\pi(Q^2)$, and to the highest value for the ratio $F_\pi^{(1)}(Q^2)/F_\pi^{(0)}(Q^2)$. In contrast to that, the choice of the BLM scale, represented by the dashed-dotted curve, leads to somewhat higher values of $Q^2F_\pi(Q^2)$, but to considerably lower values of the ratio $F_\pi^{(1)}(Q^2)/F_\pi^{(0)}(Q^2)$.

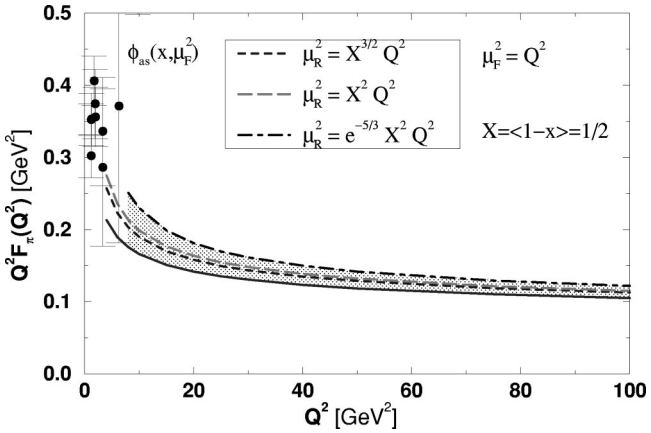

FIG. 13. Leading-twist NLO QCD results for $Q^2F_\pi(Q^2)$ obtained with the $\phi_{as}(x,\mu_F^2)$ distribution amplitude and the choices of μ_R^2 given by Eq. (4.19), with $\mu_F^2=Q^2$ and $\langle\overline{x}\rangle_{as}=1/2$. The solid curve (included for comparison) corresponds to the case $\mu_R^2=\mu_F^2=Q^2$ considered in the preceding subsection. The shaded area denotes the range of the total NLO prediction $Q^2F_\pi(Q^2)$ where the upper limit corresponds to $\mu_R^2=\mu_{PMS}^2$ obtained from Eq. (5.11).

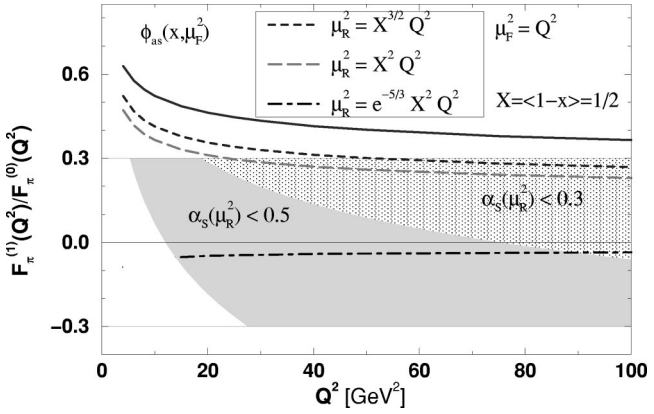

FIG. 14. The ratio $F_\pi^{(1)}(Q^2)/F_\pi^{(0)}(Q^2)$ obtained with the $\phi_{as}(x,\mu_F^2)$ distribution amplitude and the choices of μ_R^2 given by Eq. (4.19), with $\mu_F^2=Q^2$ and $\langle\overline{x}\rangle_{as}=1/2$. The solid curve (included for comparison) is for the result corresponding to $\mu_R^2=\mu_F^2=Q^2$ obtained in the preceding subsection, and the shaded area denotes the region of the predictions which correspond to $\alpha_S(\mu_R^2)<0.5$ ($\alpha_S(\mu_R^2)<0.3$), while $|F_\pi^{(1)}(Q^2)/F_\pi^{(0)}(Q^2)|<0.3$.

Adopting the previously stated criteria, we now comment on the reliability of the NLO predictions for $Q^2F_\pi(Q^2)$ displayed in Figs. 13 and 16. Imposing the requirements $|F_\pi^{(1)}(Q^2)/F_\pi^{(0)}(Q^2)|<0.3$, and $\alpha_S(\mu_R^2)<0.3$, we find from Fig. 14 that for the $\phi_{as}(x,\mu_F^2)$ distribution the results corresponding to $a=\langle\overline{x}\rangle^{3/2}$, $\langle\overline{x}\rangle^2$, and $e^{-5/3}\langle\overline{x}\rangle^2$, become reliable for the momentum transfer $Q^2>50$, 25, and 90 GeV^2, respectively. The requirement $\alpha_S(\mu_R^2)<0.3$ might be (unnecessarily) too stringent. Thus, by relaxing it and taking $\alpha_S(\mu_R^2)<0.5$ instead, we find that the results corresponding to $a=\langle\overline{x}\rangle^{3/2}$, $\langle\overline{x}\rangle^2$, and $e^{-5/3}\langle\overline{x}\rangle^2$, become reliable for the momentum transfer $Q^2>50$, 25, and 15 GeV^2, respectively.

Applying the same criteria to the case of the $\phi_{CZ}(x,\mu_R^2)$ distribution, we find from Fig. 17 that the results for

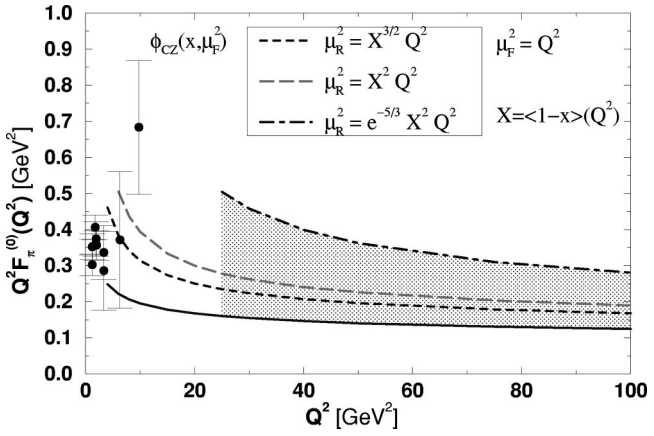

FIG. 15. The numerical results for $Q^2F_\pi^{(0)}(Q^2)$ obtained with the $\phi_{CZ}(x,\mu_F^2)$ distribution amplitude and the choices of μ_R^2 given by Eq. (4.19), with $\mu_F^2=Q^2$ and $\langle\overline{x}\rangle_{CZ}(Q^2)$ calculated according to Eq. (4.23). The solid curve (included for comparison) corresponds to the case $\mu_R^2=\mu_F^2=Q^2$ considered in the preceding subsection. The shaded area denotes the range of the LO prediction $Q^2F_\pi^{(0)}(Q^2)$ for $\mu_R^2/Q^2\in[e^{-5/3}\langle\overline{x}\rangle^2,1]$.

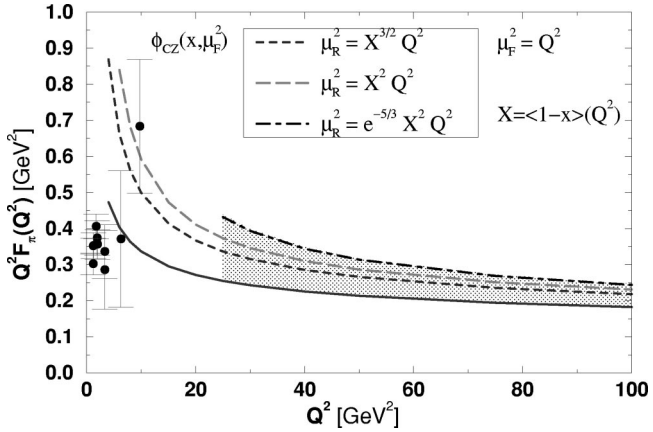

FIG. 16. Leading-twist NLO QCD results for $Q^2F_\pi(Q^2)$ obtained with the $\phi_{CZ}(x,\mu_F^2)$ distribution amplitude and the choices of μ_R^2 given by Eq. (4.19), with $\mu_F^2=Q^2$ and $\langle\overline{x}\rangle_{CZ}(Q^2)$ calculated according to Eq. (4.23). The solid curve (included for comparison) corresponds to the case $\mu_R^2=\mu_F^2=Q^2$ considered in the preceding subsection. The shaded area denotes the range of the total NLO prediction $Q^2F_\pi(Q^2)$ where the upper limit corresponds to $\mu_R^2=\mu_{PMS}^2$ obtained from Eq. (5.11).

$Q^2F_\pi(Q^2)$, shown in Fig. 16, obtained with $a=\langle\overline{x}\rangle^{3/2}$, $\langle\overline{x}\rangle^2$, and $e^{-5/3}\langle\overline{x}\rangle^2$, become reliable for the momentum transfer $Q^2>95$, 60, and 300 GeV^2, respectively, if we demand that $\alpha_S(\mu_R^2)<0.3$, and for $Q^2>95$, 35, and 50 GeV^2, respectively, if $\alpha_S(\mu_R^2)<0.5$ is regarded as a stringent enough requirement.

Summarizing the above, one can say that contrary to the rather high value of $Q^2\approx500$ GeV^2 required to obtain a reliable prediction assuming the $\phi_{as}(x,\mu_R^2)$ distribution with $\mu_R^2=Q^2$, one finds that by choosing the renormalization scale determined by the dynamics of the pion rescattering

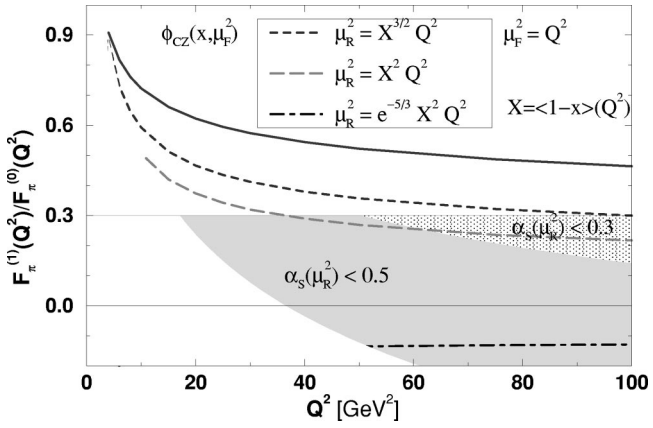

FIG. 17. The ratio $F_\pi^{(1)}(Q^2)/F_\pi^{(0)}(Q^2)$ obtained with the $\phi_{CZ}(x,\mu_F^2)$ distribution amplitude and the choices of μ_R^2 given by Eq. (4.19), with $\mu_F^2=Q^2$ and $\langle\overline{x}\rangle_{CZ}(Q^2)$ calculated according to Eq. (4.23). The solid curve (included for comparison) is for the result corresponding to $\mu_R^2=\mu_F^2=Q^2$ obtained in the preceding subsection, and the shaded area denotes the region of the predictions which correspond to $\alpha_S(\mu_R^2)<0.5$ ($\alpha_S(\mu_R^2)<0.3$), while $|F_\pi^{(1)}(Q^2)/F_\pi^{(0)}(Q^2)|<0.3$.

process, the size of the NLO corrections is significantly reduced and reliable predictions are obtained at considerably lower values of Q^2, namely, for $Q^2<100\ \mathrm{GeV}^2$. The same conclusion also applies to the results obtained with the $\phi_{CZ}(x,\mu_R^2)$ distribution, for which choosing the renormalization scale related to the virtuality of the particles in the parton subprocess lowers the bound of the reliability of the results from $Q^2\approx 2400\ \mathrm{GeV}^2$ to $Q^2<100\ \mathrm{GeV}^2$.

2. Theoretical uncertainty of the NLO predictions related to the renormalization scale ambiguity

Unfortunately, at present we do not have at our disposal any absolutely reliable method of determining the ''optimal'' (or ''correct'') value of the renormalization scale for any particular order of PQCD. Our ignorance concerning the ''optimal'' value for μ_R implies that any particular choice of this scale leads to an intrinsic theoretical uncertainty (error) of the perturbative results. Therefore, the NLO results displayed in Figs. 13 and 16, being obtained with the four singled-out values of the renormalization scale μ_R, contain theoretical uncertainty. In what follows we try to estimate this uncertainty. In order to do that, we have to make some assumptions, regarding the range of the renormalization scale ambiguity.

As already mentioned, in addition to the BLM method, two more renormalization scale-setting methods have been proposed: the FAC and PMS methods. All three of them are somewhat ad hoc and have no strong justification. Nevertheless, the principles underlying these methods are plausible, so that they give us at least a range of scale μ_R which should be considered.

Let μ_{FAC}, μ_{PMS}, and μ_{BLM} designate the scales determined by the FAC, PMS, and BLM scale-setting methods, respectively.

According to the FAC procedure, the scale μ_R is determined by the requirement that the NLO coefficient in the perturbative expansion of $F_\pi(Q^2)$ vanishes, which, in our case, effectively reduces to solving the equation

$$F_\pi^{(1)}(Q^2,\mu_R^2=\mu_{FAC}^2)=0. \tag{5.10}$$

On the other hand, in the PMS procedure, one chooses the renormalization scale μ_R at the stationary point of the truncated perturbative series for $F_\pi(Q^2)$. Operationally, this amounts to

$$\left.\frac{dF_\pi(Q^2,\mu_R^2)}{d\mu_R^2}\right|_{\mu_R^2=\mu_{PMS}^2}=0. \tag{5.11}$$

The BLM-determined scale is given by

$$\mu_{BLM}^2=e^{-5/3}\langle\overline{x}\rangle^2 Q^2. \tag{5.12}$$

The explicit expressions for $F_\pi(Q^2)$ and $F_\pi^{(1)}(Q^2)$ are given by Eqs. (5.3)–(5.7) with $\mu_F^2=Q^2$. By solving Eqs. (5.10) and (5.11), and taking Eq. (5.12) into account we find that for the $\phi_{as}(x,\mu_F^2)$ distribution

$$\mu_{BLM}^2=Q^2/21, \tag{5.13a}$$

$$\mu_{PMS}^2\approx Q^2/18, \tag{5.13b}$$

$$\mu_{FAC}^2\approx Q^2/18, \tag{5.13c}$$

while, for the $\phi_{CZ}(x,\mu_F^2)$ distribution,

$$Q^2/79<\mu_{BLM}^2<Q^2/77, \tag{5.14a}$$

$$Q^2/59<\mu_{PMS}^2<Q^2/54, \tag{5.14b}$$

$$Q^2/53<\mu_{FAC}^2<Q^2/48, \tag{5.14c}$$

for $50\ \mathrm{GeV}^2<Q^2<100\ \mathrm{GeV}^2$. Therefore, we find that for both distributions

$$\mu_{BLM}^2<\mu_{PMS}^2<\mu_{FAC}^2. \tag{5.15}$$

The FAC, PMS, and BLM scales, as evident from Eqs. (5.13) and (5.14), are very close to each other, and the curves corresponding to the NLO prediction for $Q^2F_\pi(Q^2)$ obtained with the FAC and PMS scales practically coincide with the dashed-dotted curves in Figs. 13 and 16 corresponding to the BLM scale.

If the renormalization scale is interpreted as a ''typical'' scale of virtual momenta in the corresponding Feynman diagrams, then, despite the fact that we do not know what the ''optimal'' value of this scale is, it is (based on physical grounds and on the above considerations) reasonable to assume that it belongs to the interval ranging from μ_{BLM}^2 to Q^2. Namely, μ_{BLM}^2, being the lowest of the above considered scales and of the order of $Q^2/21$ and $Q^2/80$ for the $\phi_{as}(x,\mu_F^2)$ and $\phi_{CZ}(x,\mu_F^2)$ distributions, respectively, is a low enough to serve as the lower limit of the renormalization scale ambiguity interval. On the other hand, Q^2 is (too) high a scale, and as such can safely be used for the upper limit of the same interval.

In the following, then, instead of using any singled-out value, we vary the renormalization scale in the form

$$\mu_R^2=aQ^2, \tag{5.16a}$$

where a is a continuous parameter

$$a\in[e^{-5/3}\langle\overline{x}\rangle^2,1]. \tag{5.16b}$$

Doing this will enable us to draw some qualitative conclusions concerning, first, the theoretical uncertainty related to the renormalization scale ambiguity, and, second, the effects that the inclusion of the NLO corrections has on the LO predictions.

The LO result for the pion form factor is a monotonous function of the renormalization scale μ_R. Namely, all of the μ_R dependence of the LO prediction $Q^2F_\pi^{(0)}(Q^2)$, as it is seen from Eq. (5.3), is contained in the strong coupling constant $\alpha_S(\mu_R^2)$. Thus, in accordance with Eq. (2.2), as μ_R decreases the LO result increases, and it increases without bound. In contrast to the LO, the NLO contribution $Q^2F_\pi^{(1)}(Q^2)$, as evident from the explicit expression given in

Eq. (5.5), decreases (becomes more negative) with decreasing μ_R. Upon adding up the LO and NLO contributions, we find that the full NLO result, as a function of μ_R stabilizes and reaches a maximum value for $\mu_R^2=\mu_{PMS}^2$. The values of the scale μ_{PMS} are, for the $\phi_{as}(x,Q^2)$ and $\phi_{CZ}(x,Q^2)$ distributions given by Eqs. (5.13b) and (5.14b), respectively.

If the renormalization scale continuously changes in the interval defined by Eq. (5.16), we find that the curves representing the LO and NLO results for $Q^2F_\pi(Q^2)$ fill out the shaded regions in Figs. 12 and 13, for the $\phi_{as}(x,Q^2)$, and in Figs. 15 and 16 for the $\phi_{CZ}(x,Q^2)$ distribution.

Next we turn to discuss the intrinsic theoretical uncertainty of the NLO prediction related to the renormalization scale ambiguity. Regarding this uncertainty, there is in fact no consensus on how to estimate it, or how to identify what the central value of $Q^2F_\pi(Q^2)$ should be.

Nevertheless, the simplest but still a good measure of this uncertainty is the quantity

$$\Delta F_\pi(Q^2,\mu_{min}^2,\mu_{max}^2)=Q^2F_\pi(Q^2,\mu_{min}^2) - Q^2F_\pi(Q^2,\mu_{max}^2), \quad (5.17)$$

i.e., the difference of the results for $Q^2F_\pi(Q^2)$ corresponding to the lower (μ_{min}) and the upper limit (μ_{max}) of the renormalization scale ambiguity interval (5.16). This quantity, therefore, for a given value of Q^2, represents the ''width'' of the shaded regions in Figs. 12, 13, 15, and 16. In this sense, the shaded regions in these figures, limited by the curves corresponding to $\mu_R^2=Q^2$ and $\mu_R^2=\mu_{BLM}^2$, essentially determine the theoretical accuracy allowed by the LO and NLO calculations.

A glance at Figs. 12 and 13, displaying the LO and NLO predictions for $Q^2F_\pi(Q^2)$ calculated with the $\phi_{as}(x,Q^2)$ distribution, reveals that, compared to the LO, the NLO results exibit a much smaller renormalization scale dependence. The same holds true for the predictions depicted in Figs. 15 and 16, based on the $\phi_{CZ}(x,Q^2)$ distribution.

To be more quantitative, we thus find that, if, for the $\phi_{as}(x,Q^2)$ distribution, at $Q^2=50$ GeV^2 (100 GeV^2), instead of $\mu_R^2=Q^2$ one takes $\mu_R^2=\mu_{BLM}^2=Q^2/21$, the LO result (Fig. 12) increases by 75% (64%), whereas the NLO result (Fig. 13) increases by 20% (16%). Analogously, for the same values of Q^2, but for the $\phi_{CZ}(x,Q^2)$ distribution we find that taking $\mu_R^2=\mu_{BLM}^2\approx Q^2/79$ instead $\mu_R^2=Q^2$ the LO result increases by 158% (125%), while the NLO result increases by 47% (34%).

Therefore, the NLO corrections improve the situation because the terms in the NLO hard-scattering amplitude arise such that they cancel part of the scale dependence of the LO result.

It should be pointed out that our estimate of the renormalization scale ambiguity interval given in Eq. (5.16) is very conservative, overestimating the theoretical uncertainty of the calculated NLO predictions. Namely, one could, almost at no risk, replace Q^2 by $\langle x\rangle^{3/2}Q^2$ as the upper limit of the interval. If this is done, the dotted rather than solid curves would then provide the lower bound of the shaded regions in Figs. 13 and 16. Then, for $Q^2\geqslant 50$ GeV^2 theoretical uncertainty of the NLO result for $Q^2F_\pi(Q^2)$ turns out to be less than 5% for the $\phi_{as}(x,Q^2)$ and 8% for the $\phi_{CZ}(x,Q^2)$ distribution.

Before closing this subsection, a remark is appropriate. If the shaded areas in Figs. 13 and 16 are displayed in the same figure they would not overlap. This implies that an unambiguous discrimination between the $\phi_{as}(x,Q^2)$ and $\phi_{CZ}(x,Q^2)$ distributions is possible, as soon as the data extending to higher values of Q^2 are obtained.

Based on the above considerations, we may conclude that the inclusion of the NLO corrections stabilizes the LO prediction for the pion form factor by considerably reducing the intrinsic theoretical uncertainty related to the renormalization scale ambiguity. This uncertainty for both distributions turns out to be less than 10%.

VI. SUMMARY AND CONCLUSIONS

In this paper we have presented the results of a complete leading-twist NLO QCD analysis of the spacelike electromagnetic form factor of the pion at large momentum transfer Q.

To clarify the discrepancies in the analytical expression for the hard-scattering amplitude present in previous calculations, we have carefully recalculated the one-loop Feynman diagrams shown in Fig. 3. Working in the $\overline{\rm MS}$ renormalization scheme and employing the dimensional regularization method to treat all divergences (UV, IR, and collinear), we have obtained results which are in agreement with those of Refs. [5] (up to the typographical errors listed in [9]) and [7].

As nonperturbative input at the reference momentum scale of 0.5 GeV, we have used the four available pion distribution amplitudes defined by Eq. (3.24) and plotted in Fig. 5: the asymptotic distribution $\phi_{as}(x,\mu_F^2)$ and the three QCD sum-rule inspired distributions $\phi_{CZ}(x,\mu_F^2)$, $\phi_{P2}(x,\mu_F^2)$, and $\phi_{P3}(x,\mu_F^2)$. The NLO evolution of these distributions has been determined using the formalism developed in Ref. [20].

By convoluting, according to Eq. (1.1), the hard-scattering amplitude with the pion distribution amplitude, both calculated in the NLO approximation, we have obtained the NLO numerical predictions for the pion form factor, for the four candidate distributions, and for several different choices of the renormalization and factorization scales, μ_R and μ_F. All the predictions have been obtained assuming $n_f=3$ and $\Lambda_{\overline{\rm MS}}=0.2$ GeV. We adopt the criteria according to which NLO prediction is considered reliable if, both, the ratio of the NLO to LO contributions and the strong coupling constant are reasonably small.

We have first used the most simple choice of the scales where $\mu_R^2=\mu_F^2=Q^2$. The results are summarized in Figs. 8 and 9 and Tables II–V. Our numerical results based on the asymptotic distribution amplitude $\phi_{as}(x,\mu_F^2)$ differ from those of Ref. [5] (the difference is due to the different value of $\Lambda_{\overline{\rm MS}}$). Thus, in contrast to Ref. [5], where it was concluded that ''reliable perturbative predictions cannot be made until momentum transfers Q of about 100 GeV are

reached,'' we have found that reliable predictions can already be made at momentum transfers of the order of 25 GeV. It has been shown that the inclusion of the (NLO) evolutional corrections only slightly influences the NLO prediction obtained assuming the $\phi_{as}(x,\mu_F^2)$ distribution. On the other hand, for the case of the end-point concentrated distributions, the evolutional corrections, both the LO and the NLO, are important. For the $\mu_R^2=\mu_F^2=Q^2$ choice of scales, the NLO corrections based on the $\phi_{as}(x,\mu_F^2)$, $\phi_{CZ}(x,\mu_F^2)$ $\phi_{P2}(x,\mu_F^2)$, and $\phi_{P3}(x,\mu_F^2)$ distributions, are large, which implies that one must demand that the momentum transfer Q be considerably larger than 10 GeV before the corresponding results become reliable.

In order to reduce the size of the NLO corrections and to examine the extent to which the NLO predictions for the pion form factor depend on the scales μ_R and μ_F, in addition to the simplest choice $\mu_R^2=\mu_F^2=Q^2$ (which certainly is not best suited for the process of interest), we have also considered the choices of μ_R and μ_F given by Eqs. (4.19) and (4.20), respectively. Compared to the μ_R dependence, the μ_F dependence of the results turns out to be of secondary importance. Making use of the physically motivated choices for μ_R (related to the average virtuality of the particles in the parton subprocess), and modeling the pion with the $\phi_{as}(x,\mu_F^2)$ and $\phi_{CZ}(x,\mu_F^2)$ distribution amplitudes, leads to the predictions shown in Figs. 13, 14, 16, and 17. The $\phi_{P2}(x,\mu_F^2)$ and $\phi_{P3}(x,\mu_F^2)$ distributions are not separately considered, since the corresponding results are very similar to those obtained with $\phi_{CZ}(x,\mu_F^2)$.

For a given distribution amplitude, the values of the pion form factor $Q^2F_\pi(Q^2)$ are very stable against the variation of the renormalization scale μ_R. This is evident from Figs. 13 and 16, and is a reflection of the stabilizing effect that the inclusion of the NLO corrections has on the LO predictions. On the other hand, the ratio of the NLO corrections to the LO prediction, $F_\pi^{(1)}(Q^2)/F_\pi^{(0)}(Q^2)$ is very sensitive to the values of μ_R, as can be seen from Figs. 14 and 17. Requiring this ratio to be less than 0.3 and taking the less stringent condition on the value of the strong coupling $\alpha_S(\mu_R^2)<0.5$, we find that the reliable predictions can already be made for the momentum transfer Q of the order $5-10$ GeV.

Given the fact that we do not know what the ''optimal'' value of the renormalization scale is, choosing any particular value for this scale introduces a theoretical uncertainty in the NLO predictions. Based on a reasonable guess about the renormalization scale ambiguity interval, we have estimated this uncertainty to be less than 10%.

The difference between the absolute predictions based on the $\phi_{as}(x,\mu_F^2)$, $\phi_{CZ}(x,\mu_F^2)$ $(\phi_{P2}(x,\mu_F^2))$, and $\phi_{P3}(x,\mu_F^2)$ distributions is large enough to allow an unambiguous experimental discrimination between them, as soon as the data extending to higher values of Q become available.

In conclusion, the results of the complete leading-twist NLO QCD analysis, which has been carried out in this paper, show that reliable perturbative predictions for the pion electromagnetic form factor with all distribution amplitudes considered can already be made at a momentum transfer Q of the order of $5-10$ GeV, with corrections to the LO results being up to 30%. Theoretical uncertainty related to the renormalization scale ambiguity, which constitutes a reasonable range of physical values, has been estimated to be less than 10%. To check our predictions and to choose between the distribution amplitudes, it is necessary that experimental data at higher values of Q^2 are obtained.

ACKNOWLEDGMENTS

The authors would like to thank A. V. Radyushkin for pointing out an error present in the original version of the manuscript, and P. Kroll for useful suggestions. This work was supported by the Ministry of Science and Technology of the Republic of Croatia under Contract No. 00980102.

[1] S. J. Brodsky and G. P. Lepage, Phys. Lett. **87B**, 359 (1979); G. P. Lepage and S. J. Brodsky, Phys. Rev. Lett. **43**, 545 (1979); **43**, 1625(E) (1979); Phys. Rev. D **22**, 2157 (1980).

[2] A. V. Efremov and A. V. Radyushkin, Theor. Math. Phys. **42**, 97 (1980); Phys. Lett. **94B**, 245 (1980).

[3] A. Duncan and A. H. Mueller, Phys. Lett. **90B**, 159 (1980); Phys. Rev. D **21**, 1636 (1980).

[4] S. J. Brodsky and G. P. Lepage, in *Perturbative QCD*, edited by A. H. Mueller (World Scientific, Singapore, 1989); V. L. Chernyak, in *High p_T Physics and Higher Twists*, Proceedings of the Conference, Paris, France, 1988, edited by M. Benayoun, M. Fontannaz, and J. L. Narjoux [Nucl. Phys. B (Proc. Suppl.) (Proc. Suppl.) **7B**, 297 (1989)].

[5] R. D. Field, R. Gupta, S. Otto, and L. Chang, Nucl. Phys. **B186**, 429 (1981).

[6] F.-M. Dittes and A. V. Radyushkin, Yad. Fiz. **34**, 529 (1981) [Sov. J. Nucl. Phys. **34**, 293 (1981)].

[7] M. H. Sarmadi, Ph.D. thesis, University of Pittsburgh, 1982.

[8] R. S. Khalmuradov and A. V. Radyushkin, Yad. Fiz. **42**, 458 (1985) [Sov. J. Nucl. Phys. **42**, 289 (1985)].

[9] E. Braaten and S.-M. Tse, Phys. Rev. D **35**, 2255 (1987).

[10] E. P. Kadantseva, S. V. Mikhailov, and A. V. Radyushkin, Yad. Fiz. **44**, 507 (1986) [Sov. J. Nucl. Phys. **44**, 326 (1986)].

[11] F. D. Aguila and M. K. Chase, Nucl. Phys. **B193**, 517 (1981).

[12] E. Braaten, Phys. Rev. D **28**, 524 (1983).

[13] B. Nižić, Phys. Rev. D **35**, 80 (1987).

[14] N. Isgur and C. H. Llewellyn Smith, Phys. Rev. Lett. **52**, 1080 (1984); Phys. Lett. B **217**, 535 (1989); Nucl. Phys. **B317**, 526 (1989).

[15] A. V. Radyushkin, Nucl. Phys. **A532**, 141 (1991).

[16] H.-N. Li and G. Sterman, Nucl. Phys. **B381**, 129 (1992); D. Tung and H.-N. Li, Chin. J. Phys. **35**, 651 (1997).

[17] R. Jakob and P. Kroll, Phys. Lett. B **315**, 463 (1993); **319**, 545(E) (1993).

[18] F.-M. Dittes and A. V. Radyushkin, Phys. Lett. **134B**, 359 (1984); M. H. Sarmadi, *ibid.* **143B**, 471 (1984); G. R. Katz, Phys. Rev. D **31**, 652 (1985); S. V. Mikhailov and A. V. Radyushkin, Nucl. Phys. **B254**, 89 (1985).

[19] S. V. Mikhailov and A. V. Radyushkin, Nucl. Phys. **B273**, 297 (1986).
[20] D. Müller, Phys. Rev. D **49**, 2525 (1994); **51**, 3855 (1995).
[21] G. Curci, W. Furmanski, and R. Petronzio, Nucl. Phys. **B175**, 27 (1980).
[22] S. J. Brodsky, P. Damgaard, Y. Frishman, and G. P. Lepage, Phys. Rev. D **33**, 1881 (1986).
[23] V. L. Chernyak and A. R. Zhitnitsky, Phys. Rep. **112**, 173 (1984).
[24] G. Martinelli and C. Sacharadja, Phys. Lett. B **190**, 151 (1987); **217**, 319 (1989).
[25] E. G. Floratos, D. A. Ross, and C. T. Sachrajda, Nucl. Phys. **B129**, 66 (1977); **B139**, 545(E) (1978).
[26] A. Gonzales-Arroyo, C. Lopez, and F. J. Yndurain, Nucl. Phys. **B153**, 161 (1979).
[27] G. R. Farrar, K. Huleihel, and H. Zhang, Nucl. Phys. **B349**, 655 (1991).
[28] S. J. Brodsky, G. P. Lepage, and P. B. Mackenzie, Phys. Rev. D **28**, 228 (1983).
[29] G. Grunberg, Phys. Lett. **95B**, 70 (1980); **110B**, 501 (1982); Phys. Rev. D **29**, 2315 (1984).
[30] P. M. Stevenson, Phys. Lett. **100B**, 61 (1981); Phys. Rev. D **23**, 2916 (1981); Nucl. Phys. **B203**, 472 (1982); **B231**, 65 (1984).
[31] G. Kramer and B. Lampe, Z. Phys. A **339**, 189 (1991).
[32] G. Parisi and R. Petronzio, Phys. Lett. **94B**, 51 (1980); A. C. Mattingly and P. M. Stevenson, Phys. Rev. D **49**, 437 (1994); V. N. Gribov, Lund Report No. LU-TP 91-7, 1991 (unpublished); K. D. Born, E. Laermann, R. Sommer, P. M. Zerwas, and T. F. Walsh, Phys. Lett. B **329**, 325 (1994); J. M. Cornwall, Phys. Rev. D **26**, 1453 (1982); A. Donnachie and P. V. Landshoff, Nucl. Phys. **B311**, 509 (1989); M. B. Gay Ducati, F. Halzen, and A. A. Natale, Phys. Rev. D **48**, 2324 (1993).
[33] S. Peris and E. de Rafael, Nucl. Phys. **B500**, 325 (1997).
[34] C. J. Bebek *et al.*, Phys. Rev. D **17**, 1693 (1978).
[35] S. R. Amendolia *et al.*, Nucl. Phys. **B277**, 168 (1986).
[36] C. E. Carlson and J. Milana, Phys. Rev. Lett. **65**, 1717 (1990).
[37] S. Dubnička and L. Martinovič, Phys. Rev. D **39**, 2079 (1989); J. Phys. G **15**, 1349 (1989).
[38] A. V. Radyushkin, Acta Phys. Pol. B **26**, 2067 (1995); S. Ong, Phys. Rev. D **52**, 3111 (1995); P. Kroll and M. Raulfs, Phys. Lett. B **387**, 848 (1996).